Research Square

Preprints are preliminary reports that have not undergone peer review.
They should not be considered conclusive, used to inform clinical practice,
or referenced by the media as validated information.

A Novel Synbiotics-Lactobacillus - ML/MN/T2/T23/TF from Ethanol-Tolerant Healthy Individuals in Combination with Sodium Butyrate Alleviates Alcoholic Liver Disease by Restoring the Homeostasis of Gut-Liver Axis

Feiyan Long
General Hospital, First Clinical Medical College, Ningxia Medical University, Yinchuan 750004
Jinyu Li
General Hospital, First Clinical Medical College, Ningxia Medical University, Yinchuan 750004
Yanru Kang
General Hospital, First Clinical Medical College, Ningxia Medical University, Yinchuan 750004
Yanjing Li
General Hospital, First Clinical Medical College, Ningxia Medical University, Yinchuan 750004
Tian Ma
General Hospital, First Clinical Medical College, Ningxia Medical University, Yinchuan 750004
Junbai Ma
Ningxia Key Laboratory of Infection and Immunity, School of Basic Medical Sciences, Ningxia Medical University, Yinchuan 750004
Jian Liu
Ningxia Key Laboratory of Infection and Immunity, School of Basic Medical Sciences, Ningxia Medical University, Yinchuan 750004
Ping Yang
General Hospital, First Clinical Medical College, Ningxia Medical University, Yinchuan 750004
Shuai Luo
General Hospital, First Clinical Medical College, Ningxia Medical University, Yinchuan 750004
Lina Zhang
General Hospital, First Clinical Medical College, Ningxia Medical University, Yinchuan 750004
Xiaoxia Zhang
College of Traditional Chinese Medicine, Ningxia Medical University, Yinchuan 750004
Shaoqi Yang
General Hospital, First Clinical Medical College, Ningxia Medical University, Yinchuan 750004

Hao Wang

wanghaograduate@126.com

Ningxia Key Laboratory of Infection and Immunity, School of Basic Medical Sciences, Ningxia Medical University, Yinchuan 750004

Research Article

Keywords: Alcoholic liver disease, Ethanol-metabolizing bacterial strain, Butyrate, Synbiotics, Inflammation

Posted Date: May 28th, 2026

DOI: https://doi.org/10.21203/rs.3.rs-9739470/v1

License: This work is licensed under a Creative Commons Attribution 4.0 International License. Read Full License

Additional Declarations: No competing interests reported.

A Novel Synbiotics-*Lactobacillus -ML/MN/T2/T23/TF* from Ethanol-Tolerant Healthy Individuals in Combination with Sodium Butyrate Alleviates Alcoholic Liver Disease by Restoring the Homeostasis of Gut-Liver Axis

Feiyan Long[1#], Jinyu Li[1#], Yanru Kang[1], Yanjing Li[1], Tian Ma[1], Junbai Ma[2], Jian Liu[2], Ping Yang[1], Shuai Luo[1], Lina Zhang[1], Xiaoxia Zhang[3*], Shaoqi Yang[1*], Hao Wang[2*]

1. General Hospital, First Clinical Medical College, Ningxia Medical University, Yinchuan 750004, China;

2. Ningxia Key Laboratory of Infection and Immunity, School of Basic Medical Sciences, Ningxia Medical University, Yinchuan 750004, China;

3. College of Traditional Chinese Medicine, Ningxia Medical University, Yinchuan 750004, China.

# These authors contributed equally to this work.

* Corresponding authors.

E-mail address: zxx1216@163.com (Xiaoxia Zhang), shaoqiynh@163.com (Shaoqi Yang), wanghaograduate@126.com (Hao Wang).

Abstract

Objective: Alcoholic liver disease (ALD) resulting from sustained excessive alcohol consumption is a leading global cause of chronic liver injury, characterized by persistent hepatic inflammation and profound gut microbiota dysbiosis. Despite its substantial burden of morbidity and mortality, no effective therapeutic interventions are currently available beyond alcohol abstinence. Therefore, this study aims to investigate the ameliorative effects of probiotic strains with ethanol-metabolizing capacity, administered either alone or in combination with beneficial microbiota-derived metabolite sodium butyrate (NaB) on ALD.

Methods: Probiotic strains representing capable of ethanol metabolism were isolated, purified, and identified from individuals with long-term alcohol consumption but without liver injury. These

strains were then administered individually or in combination with NaB in antibiotic cocktail (ABX)-treated C57BL/6J mice fed an ethanol-containing Lieber-DeCarli liquid diet. After 6 weeks of treatment, mice were euthanized and relevant parameters were investigated.

Results: We isolated 14 ethanol-metabolizing bacterial strains from fecal samples of healthy individuals with chronic heavy alcohol consumption. Intriguingly, five of the 14 candidate probiotic strains, namely ML, MN, T2, T23, and TF, exhibited significantly enhanced growth during *in vitro* co-culture with NaB. Administration of each of these strains markedly attenuated hepatic steatosis in ALD mice, as evidenced by reduced serum concentrations of triglycerides (TG) and low-density lipoprotein (LDL), alonged with decreased activities of alanine aminotransferase (ALT) and aspartate aminotransferase (AST). Furthermore, these probiotics suppressed inflammation by reducing pro-inflammatory tumor necrosis factor-alpha (TNF-α), interleukin (IL)-6, IL-1β, and elevating anti-inflammatory IL-10. Importantly, the stranis separately improved ethanol clearance via enhancing both activity and expression of alcohol dehydrogenase (ADH) and aldehyde dehydrogenase (ALDH). Moreover, the combination of each strain of these five strains with NaB yielded significantly greater improvements across ALD-related pathological parameters than those in probiotic monotherapy, demonstrating a robust synergistic therapeutic effect. Metagenomic analysis further revealed that these strains were markedly enriched in metabolic pathways including central to glycolysis, pyruvate metabolism, and the glyoxylate cycle.

Conclusion: This study provides a novel synbiotics of five probiotic strains in combination with NaB possessing ethanol-metabolizing capacity, which may contribute to potential preventive and therapeutic agents for ALD.

Keyword: Alcoholic liver disease; Ethanol-metabolizing bacterial strain; Butyrate; Synbiotics; Inflammation

Introduction

ALD is a progressive hepatic injury resulting from chronic excessive alcohol consumption, probably leading to steatohepatitis, fibrosis, cirrhosis, and ultimately hepatocellular carcinoma [1, 2]. ALD and related complications account for 5.3% of global mortality, among which the diagnosis at intermediate-to-advanced stages, the 5-year survival rate remains below 40%[3-5]. Although liver

transplantation represents the only effective therapeutic option for end-stage disease, its clinical application is severely limited by a substantial donor organ shortage and graft survival rates that remain suboptimal falling short of 80%[6, 7]. These constraints underscore an urgent need for innovative strategies and breakthrough therapeutic interventions.

Advances in research on the gut–liver axis have underscored the pivotal role of the gut microbiota that represents a highly complex and dynamic ecosystem in nutrient provision, metabolic regulation, and immune regulation[8]. Dysbiosis of the gut microbiota is currently recognized as a crucial pathogenesis in ALD. Chronic alcohol consumption compromises intestinal barrier integrity, markedly downregulating the expression of tight junction proteins such as ZO-1 and occludin. This disruption facilitates bacterial translocation and the portal influx of lipopolysaccharide (LPS) that activates the TLR4/NF-κB signaling pathway in hepatic Kupffer cells, triggering a pro-inflammatory cascade characterized by elevating TNF-α and IL-6, thereby driving hepatic injury[9]. In recent years, probiotic-based interventions targeting the gut microbiota have exhibited a promise strategy for ameliorating ALD. For instance, *Lactobacillus plantarum* and *Lactobacillus acidophilus* have been demonstrated to attenuate liver damage by enhancing short-chain fatty acids (SCFAs) production and suppressing TLR4-mediated inflammatory signaling[10, 11].

Although several alcohol-metabolic strains were *in vitro* isolated from fermented foods such as yogurt and kimchi, the probiotics currently employed in interventions for ALD and their capacity for intestinal colonization and metabolic adaptability under chronic alcohol exposure still remain limited. For clinical application, we firstly successfully isolated bacterial strains with high ethanol-metabolizing activity directly from the gut microbiota of “healthy alcohol-tolerant individuals” defined as those with long-term heavy alcohol consumption but without evidence of hepatic injury. Naturally adapted to a high-alcohol milieu, these strains may possess enhanced capabilities in preserving intestinal barrier integrity and conferring hepatoprotection, thereby representing a promising new resource for the development of targeted microbiota-based therapeutics for ALD.

SCFAs are key microbial metabolites generated through the fermentation of dietary fiber by probiotics in gut microbiota. Among them, butyrate serving as the primary energy substrate for colonic epithelial cells plays a critical role in reinforcing intestinal barrier integrity and subsequently

suppressing inflammation. Moreover, supplementation with butyrate-producing bacteria such as *Faecalibacterium prausnitzii* has been shown to significantly restore gut barrier function and attenuate hepatic injury in murine models[12]. Several teams including our lab have demonstrated NaB ameliorates ALD through multiple mechanisms including restoration of the intestinal barrier, modulation of gut microbial composition, GPR43 activation and regulation of macrophage polarization via the HDAC1/miR-155 axis [13, 14]. In particular, the synergistic effects of NaB in combination with the aforementioned ethanol-metabolizing bacterial strain recently isolated from alcohol-tolerant healthy individuals has not been systematically investigated.

In this study, we isolated and characterized with ethanol-metabolizing and butyrate-promoting probiotics strains from the gut microbiota of healthy alcohol-tolerant individuals defined as those with long-term heavy alcohol consumption, and investigated the effects of single strain therapy as well as combinational efficacy with NaB on ALD. Our findings confirm that NaB exerts hepatoprotective effects in a gut microbiota - dependent manner, further reveal a synergistic combination with NaB and the ethanol-metabolizing probiotic strain. These results provide a robust experimental basis for the rational design of a targeted synbiotic formulation of a functionally defined ethanol-metabolizing probiotic combined with NaB that represents a significant step toward precision microbiota-based interventions for ALD.

Results

1. Successful isolation of ethanol-metabolizing probiotic strains from healthy alcohol-tolerant individuals

To identify specific gut bacterial strains that could direct metablize ethanol intake, we collected fecal samples from healthy alcohol-tolerant individuals with a history of chronic alcohol consumption. We then implemented a comprehensive, systematic pipeline for the isolation, identification, and functional validation of candidate bacterial strains (Figure 1).

Following two rounds of ethanol tolerance screening, we performed preliminary species identification on 91 ethanol-tolerant candidates isolated using matrix-assisted laser desorption/ionization time-of-flight mass spectrometry (MALDI-TOF MS). As shown in Table S1

1-3, the vast majority of these isolates belonged to the genus *Lactobacillus*. Specifically, *Lactobacillus acidophilus/gassier* was identified in 61 strains, and *Lactobacillus casei/paracasei/rhamnosus* in 37 strains. A smaller number of isolates were classified as *Limosilactobacillus fermentum* (12 strains) and *Limosilactobacillus reuteri* (4 strains). Beyond *Lactobacilli*, a limited number of isolates were assigned to other taxa: six strains were identified as *Enterococcus gallinarum*, and one strain as *Escherichia coli*. Notably, despite each isolate undergoing at least three independent identification runs, a small subset yielded ambiguous results, assigning them to two closely related species. This ambiguity may reflect either genuine taxonomic proximity among certain strains or inherent limitations in the discriminatory resolution of MALDI-TOF MS for highly similar bacterial species.

To evaluate the ethanol-degrading capacity of the candidate strains, we conducted a 48-hour dynamic monitoring assay of ethanol degradation kinetics. As shown in Figure 2 and S2, the majority of isolates exhibited pronounced ethanol degradation during the initial phase (within the first 4–6 hours). Notably, strains including T23, ME, MB, M2, and MF demonstrated sustained degradation activity, achieving ethanol removal rates exceeding 40% over 48 hours, with their degradation curves plateauing thereafter. Based on the 48-hour ethanol degradation efficiency, we selected the top-performing isolates, namely MB, MD, ME, MF, ML, MN, M1C, M2, M8, M15, M16, M34, M44, M46, TF, T2, T11, T13, T21, and T23 for further characterization. All 20 strains exhibited rapid ethanol metabolism, with degradation rates > 10% at 48 hours.

2. Integrated *in vitro* and genomic analysis of fourteen ethanol-metabolizing probiotic candidates

To simulate bile salt stress encountered in the intestinal environment, we screened the viability of each strain at multiple time points (2, 4, 6, and 8 hours) under two bile salt concentrations (3% and 5%). As shown in Figure 3A and S3A, bacterial survival rates were generally comparable between the two concentrations across all time points. Intriguingly, most strains exhibited higher viability in 5% bile salt than in 3%. Nevertheless, a progressive decline in survival was observed over time for all isolates. Based on this assay, two strains including M2 and M44 with survival rates below 30% under bile salt stress were excluded from further analysis. The remaining 18 strains were

subsequently evaluated for acid tolerance by exposing them to pH 2.0 and pH 3.0 conditions. As illustrated in Figure 3B and S3B, survival rates were broadly similar between the two acidic environments. Viability was monitored at 2, 4, and 6 hours post-exposure, and strains M16, M34, M46, and T13 exhibiting poor resilience that displayed consistently low survival rates under both pH conditions were eliminated from the candidate pool.

We next subjected the 14 selected candidate strains to whole-genome shotgun metagenomic sequencing and performed comprehensive genomic analyses based on the assembled contigs, including phylogenetic reconstruction, average nucleotide identity (ANI) assessment, circular genome map visualization, and functional annotation prediction. Phylogenetic tree and ANI heatmap analyses (Figure 3C and 3D) confirmed that all candidate isolates belonged to the lactic acid bacteria (LAB) group. Within the *Lactobacillus sensu stricto* clade, strains T21, MD, T11, T2, MF, ME, and TF clustered tightly within the *L. paragasseri*/*L. gasseri* species complex. Notably, T21 shared high sequence similarity and a recent common ancestor with reference strains JCM 5343 and ATCC 33323; the remaining strains in this subgroup also resided within the same well-supported monophyletic branch, indicating strong genomic homology among them. Secondly, strain MN was unambiguously placed within the *L. rhamnosus–L. paracasei* lineage, with 100% bootstrap support, confirming its close evolutionary relationship to these two species. Within the genus *Limosilactobacillus*, strains ML, MB, M8, and M1C formed a distinct, strongly supported (100% bootstrap) clade that, although sharing a common ancestor with reference strains such as *L. oris*, did not cluster within any known species' monophyletic group, suggesting these isolates may represent a novel, closely related lineage within this genus.

ANI analysis further corroborated these phylogenetic findings. Eight strains including T21 exhibited ANI values ≥98.0% with *Lactobacillus paragasseri* JCM 5343, supporting their classification as novel isolates of this species. Strain M8 showed an ANI of 99.2% with *Limosilactobacillus oris* DSM 4864, confirming its conspecificity. Additionally, strains M15, ML, M1C, and MB displayed ANI values >97.0% with *L. oris*, in consistent with membership in the same species complex. In contrast, strain MN shared an ANI of 96.9% with *Lactobacillus rhamnosus* JCM 1136 hovering at the conventional species demarcation threshold (typically 95–

96%), suggesting it may represent a distinct taxonomic lineage warranting further classification.

Circular genome map analysis (Figure 3E and S4A) confirmed that all 14 candidate strains harbored genes encoding key enzymes involved in ethanol metabolism, including multiple subtypes of alcohol dehydrogenase (*adhA*, *adhC*, *adhE*, *adh1–3*) and aldehyde dehydrogenase (*aldA*, *aldC*, *aldE*, *ald1*), collectively forming a putative two-step enzymatic pathway for ethanol degradation. Notably, substantial inter-strain heterogeneity was observed in the composition of these gene clusters. Strains M1C, M15, ML, MB, and T21 possessed the most diverse and complete repertoires of *adh* and *ald* genes, suggesting a robust genetic capacity for the full conversion of ethanol → acetaldehyde → acetate. In contrast, strains TF, T2, T23, and M8 retained only a limited subset of core ethanol-metabolizing genes. Nevertheless, every isolate carried at least one representative member of both the *adh* and *ald* families, indicating a universal genetic potential across the cohort to participate in ethanol catabolism. These findings provide a critical genomic foundation for subsequent functional validation and the rational selection of high-efficiency ethanol-degrading probiotic candidates.

Functional annotation analyses (Figure 3F–3H and S4B-S4E) provided a multi-omics perspective on the metabolic infrastructure underpinning ethanol metabolism in the candidate strains. First, Clusters of Orthologous Groups (COG) classification revealed a pronounced emphasis on core metabolic processes particularly amino acid metabolism, carbohydrate utilization, and energy production (categories E, G, and C), indicating a robust metabolic foundation conducive to handling ethanol-derived stress. Second, Kyoto Encyclopedia of Genes and Genomes (KEGG) pathway enrichment confirmed that nearly all isolates exhibited strong representation in central carbon metabolism pathways, including glycolysis (map00010), pyruvate metabolism (map00620), and the glyoxylate and dicarboxylate cycle (map00630). Notably, strains T21, T23, and MN showed marked enrichment in the glyoxylate cycle and fatty acid degradation pathways, suggesting their capacity to activate alternative energy-generating routes to mitigate ethanol-induced toxicity. In contrast, M15 and M1C displayed heightened activity in branched-chain amino acid biosynthesis and phospholipid metabolism, potentially enhancing membrane integrity and cellular stress resilience. Third, Carbohydrate-Active enZymes (CAZy) profiling demonstrated that all strains encoded a

diverse array of glycoside hydrolases (notably GH1, GH3, GH13, and GH31), endowing them with the ability to utilize complex dietary carbohydrates as carbon sources. Moreover, strains T2, TF, ML, and ME exhibited elevated expression of auxiliary activity family 3 (AA3) enzymes that includes well-characterized alcohol oxidizing dehydrogenases involved in redox homeostasis and ethanol catabolism. Collectively, these findings indicate that, beyond harboring canonical *adh* and *aldh* genes, the candidate strains are equipped with a coordinated metabolic network encompassing energy generation, substrate flexibility, and redox regulation, thereby establishing a comprehensive functional framework that synergistically supports efficient ethanol degradation.

As shown in Figure 3I and S5, all 14 candidate strains exhibited blue–purple, rod- or short rod–shaped morphology upon Gram staining, unequivocally classifying them as Gram-positive bacteria. Notably, occasional heterogeneous or faint pink discoloration was observed in a subset of strains including M8, M1C, and MF. Such staining irregularities are not uncommon among members of the phylum *Firmicutes* and are typically attributable to variations in peptidoglycan layer thickness, growth phase, or minor fluctuations in ethanol decolorization duration during the staining procedure; these artifacts do not compromise the definitive Gram-positive classification. The predominant cellular morphology with short rods is consistent with typical lactic acid bacteria, further supporting their taxonomic assignment within this group.

3. Five probiotic candidates of the above 14 strains co-cultured with NaB markedly enhanced ehtanal elimination

Our current candidate strains, validated through *in vitro* functional assays and genomic analyses, demonstrate robust ethanol-metabolizing capabilities. Our group's previous research found that NaB can ameliorate ALD through multiple pathways. We further investigated the effects of NaB combined with bacterial strains on ethanol degradation in vitro. As shown in Figure 4 and S6, in the absence of ethanol, NaB significantly enhanced the growth of strains ML, MN, T2, T23, and TF, whereas its proliferative effect on the remaining isolates was modest. When challenged with 15% (v/v) ethanol, all strains exhibited suppressed growth; however, co-administration of NaB markedly alleviated ethanol-induced growth inhibition specifically in ML, MN, T2, T23, and TF, as evidenced by a significant recovery in OD_{600} values. In contrast, other strains showed no appreciable growth

rescue upon NaB treatment. Based on these findings, we identified ML, MN, T2, T23, and TF as the five lead candidates exhibiting synergistic responsiveness to NaB and selected for subsequent *in vivo* validation as functionally relevant probiotic strains.

4. These five probiotic candidates separately exhibits a significant hepatoprotection in mice with ALD

To evaluate the hepatoprotective potential of ethanol-metabolizing probiotic strains isolated from healthy alcohol-tolerant individuals, we administered five candidate strains ML, MN, T2, T23, and TF individually via oral gavage in a mouse model of ALD pre-treated with broad-spectrum antibiotics (ABX+ALD) (Figure 5A). As shown in Figure 5C, daily food intake did not differ significantly among experimental groups, indicating that the interventions did not appreciably alter feeding behavior. However, mice in the ABX+MOD group exhibited a significant reduction in body weight starting from week 6 compared with the ABX+CON group (Figure 5B), accompanied by elevated fasting blood glucose levels (Figure 5D) and a markedly increased liver index (Figure 5F), suggesting alcohol-induced metabolic dysregulation, impaired glucose homeostasis, and hepatic steatosis. Notably, intervention with each of the five bacterial strains partially but significantly reversed alcohol-associated body weight loss, and all markedly reduced both fasting blood glucose concentrations and the liver index relative to the ABX+MOD group, underscoring their protective metabolic effects *in vivo*.

With regard to liver injury (Figure 5G–5U), mice in the ABX+MOD group exhibited significantly elevated levels of TG, TC, LDL, AKP, and TBA in both liver tissue and serum, alonged with a marked reduction in HDL. Concurrently, serum ALT and AST activities were substantially increased, indicative of severe hepatocellular injury and pronounced hepatic lipid accumulation. Intervention with each of the 5 candidate strains significantly ameliorated these abnormalities. Specifically, all strains reduced hepatic and serum levels of TG, TC, and LDL, while restoring HDL concentrations. Moreover, they markedly suppressed the alcohol-induced elevations in ALT, AST, AKP, and TBA. Among them, strains ML and T2 demonstrated particularly consistent and robust efficacy in mitigating liver injury , highlighting their superior therapeutic potential in the context of alcohol-associated metabolic and liver dysfunction.

Analysis of inflammatory mediators (Figure 6A–6H) revealed that, compared to controls, the ABX+MOD group exhibited significantly elevated levels of pro-inflammatory cytokines including TNF-α, IL-6, and IL-1β in both liver tissue and serum, concomitant with a marked reduction in the anti-inflammatory cytokine IL-10. Administration of each of the five candidate bacterial strains effectively attenuated this dysregulated inflammatory response. Notably, strain ML demonstrated the most pronounced immunomodulatory effect, with several cytokine levels approaching those observed in the control group, thereby underscoring its superior capacity to restore immune homeostasis in the context of alcohol-induced inflammation.

With regard to ethanol-metabolizing capacity (Figure 6I–6P), mice in the ABX+MOD group exhibited significantly reduced activities of ADH and ALDH in both liver tissue and serum. Intervention with each of 5 candidate strains markedly restored hepatic ADH and ALDH enzymatic activities. Notably, strains T23 and TF also significantly enhanced serum ADH and ALDH activities compared with those in the ABX+MOD group. Intriguingly, while enzyme activities were suppressed in the ABX+MOD group, the protein levels of ADH and ALDH in liver tissue were paradoxically elevated, potentially reflecting a compensatory upregulation in response to impaired function. Among the interventions, strain MN further increased the hepatic abundance of both ADH and ALDH proteins, suggesting a distinct mechanism involving transcriptional or post-translational regulation that warrants further investigation.

Collectively, all candidate strains ameliorated alcohol-induced liver injury across multiple parameters. Among them, MN, ML, and T2 demonstrated particularly robust efficacy by significantly attenuating dysregulated lipid metabolism, suppressing hepatic inflammation, restoring liver function, and enhancing ethanol-metabolizing capacity, thereby emerging as the most promising therapeutic potential of probiotic candidates that were isolated from ethanol-tolerant healthy donors for mitigating ALD.

5. Therapeutic effects of single NaB on ALD

Preliminary *in vitro* experiments have confirmed that NaB significantly promotes the growth of five probiotic strains with ethanol-metabolizing capacity, suggesting its potential as a prebiotic for

ameliorating ALD. Building on these findings, we designed *in vivo* experiments to further evaluate the interventional effects of sodium butyrate on ALD. Subsequently, we employed an antibiotic (ABX)-treated mouse model to investigate whether its protective effects are dependent on the gut microbiota.

5.1 Therapeutic effects of NaB intervention on alcoholic liver injury in mice

In a chronic ethanol-feeding mouse model (Figure 7A), NaB treatment did not significantly ameliorate alcohol-induced hyperglycemia (Figure 7D) but successfully reversed the increased liver weight and liver-to-body-weight ratio (liver index; Figures 7E–7F), indicating a reduction in hepatic burden independent of changes in bodyweight or food intake (Figures 7B–7C). NaB intervention significantly attenuates hepatic injury and lipid metabolic disorders induced by chronic alcohol exposure (Figures 7G – 7U). Histopathological and biochemical analyses confirmed that NaB effectively reversed hepatic steatosis, reduced serum aminotransferase (ALT/AST) and lipid concentrations, and restored the balance between pro-inflammatory and anti-inflammatory cytokines (Figures 8A–8I). Mechanistic investigations revealed that NaB not only restored the activity of key ethanol-metabolizing enzymes (ADH and ALDH) to accelerate alcohol clearance (Figures 8J–8Q) but also repaired intestinal barrier integrity by upregulating colonic expression of the tight-junction proteins ZO-1 and occludin (Figures 9B–9E). This gut–liver axis modulation substantially reduced serum lipopolysaccharide (LPS) concentrations (Figure 9A), thereby interrupting the endotoxaemia-driven cascade of hepatic inflammation.)

5.2 NaB rectified alcohol-induced disruptions in gut microbial diversity and community structure

16S rRNA gene sequencing was performed to characterize the effects of NaB on the gut microbiota in a murine model of ALD. Venn diagram analysis revealed that NaB intervention reduced the number of unique operational taxonomic units (OTUs) in the ALD model group, shifting the overall microbial composition towards that of healthy controls (Figure 10A). Species accumulation and rarefaction curves confirmed adequate sequencing depth and demonstrated that NaB significantly

restored alcohol-suppressed microbial diversity and richness (Figures 10B–10D). Alpha-diversity indices indicated partial recovery of microbial complexity following NaB treatment (Figures 10E–10F). Non-metric multidimensional scaling (NMDS) and principal coordinates analysis (PCoA) showed marked structural deviation in the ALD model group, which was reversed by NaB toward a healthier configuration, with minimal perturbation to baseline microbiota (Figures 10G–10H).

At the phylum level, NaB reversed alcohol-induced depletion of *Bacteroidota* and elevated *Firmicutes*-to-*Bacteroidetes* (F/B) ratio, restoring microbial architecture toward control levels (Figures 10I – 10K). At the genus level, NaB significantly enriched beneficial taxa including *Lactobacillus* and *Bifidobacterium,* while suppressing pathogenic genera such as *Bacteroides* (Figures 10L – 10N). Differential abundance analysis and LEfSe further confirmed that NaB counteracted dysbiosis through selective enrichment of probiotic species, notably *Lactobacillus reuteri* (Figures 10O – 10S). Co-occurrence network analysis unveiled complex synergistic and antagonistic interactions within the microbiota, suggesting that NaB enhances community stability by reinforcing beneficial symbiotic networks (Figures 10T–10U). Functional prediction indicated that NaB restored the abundance of microbial aldehyde dehydrogenase (EC:1.2.1.3), a key enzyme in ethanol metabolism, and enhanced functional pathways related to carbohydrate metabolism and amino acid biosynthesis, thereby supporting host metabolic homeostasis (Figures 10V–10Y).

5.3 Correlation analysis between key gut bacterial genera and ethanol-metabolizing enzymes, inflammatory markers, and hepatic function parameters

Spearman correlation heatmap analysis revealed robust associations between gut microbial taxa and host hepatic, metabolic, and inflammatory parameters (Figures 11A – 11C). Beneficial genera including *Lactobacillus* and *Bifidobacterium* showed significant negative correlations with markers of hepatic injury (ALT, AST, TBA), dyslipidaemia (TC, TG, LDL), and pro-inflammatory cytokines (TNF-α, IL-6, IL-1β), but positive correlations with protective factors HDL, IL-10, and the activities of ethanol-metabolising enzymes (ADH and ALDH). Integrated network analysis further confirmed a strong coupling among hepatic injury, inflammatory activation, and lipid metabolic disturbance.

Moreover, impaired ethanol-metabolizing capacity was closely associated with worsening pathological indices, suggesting that NaB may synergistically ameliorate host metabolic and inflammatory status by restructuring the gut microbiota.

5.4 The hepatoprotective effects of NaB on alcoholic liver injury is critically dependent on the presence of a functional gut microbial ecosystem

By establishing a broad-spectrum antibiotic (ABX) cocktail-induced pseudo-germ-free ALD model, we demonstrated that depletion of the gut microbiota significantly abrogated the therapeutic efficacy of NaB. Compared with mice harboring an intact microbiota, the ameliorative effects of NaB on fasting blood glucose (Figure 12D) and liver index (Figures 12E–12F) were markedly constrained in the absence of a resident microbial community. Biochemical analyses revealed that although NaB partially alleviated hepatic injury and lipid metabolic dysregulation in microbiota-depleted mice, its therapeutic potency was substantially attenuated relative to controls (Figures 12G – 12U). Histopathological examination confirmed that the suppressive effects of NaB on alcohol-induced hepatic steatosis (Figure 13A) and systemic inflammatory responses (TNF-α, IL-6, IL-1β; Figures 13B–13I) were considerably compromised under microbiota-deficient conditions. Furthermore, the capacity of NaB to restore ethanol-metabolising enzyme (ADH/ALDH) activity (Figures 13J–13Q), as well as to repair colonic barrier architecture (Figure 14A) and tight junction protein (occludin/ZO-1) expression (Figures 14B – 14D), was critically dependent on the presence of a structurally and functionally intact gut microbial community.

6. Combined intervention with probiotic strains and NaB significantly enhances the therapeutic efficacy against ALD

To further elucidate the synergistic mechanisms between NaB and ethanol-metabolizing bacterial strains, we administered each of the five identified candidate strains ML, MN, T2, T23, and TF respectively or in combination with NaB (0.6 g/kg body weight/day) in a mouse model of ALD pre-treated with ABX (Figure 15A). As shown in Figure 15C, daily food intake did not differ significantly among experimental groups, thereby ruling out confounding effects related to feeding

behavior. Mice in the ABX+MOD group exhibited a significant and sustained reduction in body weight beginning at week 6 relative to the ABX+CON group, which persisted until the end of the study (Figure 15B). Both single therapy and combination interventions partially restored body weight, albeit to varying degrees. Furthermore, the ABX+MOD group displayed elevated fasting blood glucose levels (Figure 15D) and a markedly increased liver index (Figure 15F), consistent with ethanol-induced disruption of glucose homeostasis and heightened hepatic metabolic burden. Notably, although no statistically significant differences were observed between monotherapy and combination therapy groups overall, a consistent downward trend in fasting glucose was evident across all combination regimens. Among them, the T2 + NaB co-administration group showed the most pronounced reduction in blood glucose compared with T2 monotherapy, suggesting a potentially enhanced metabolic benefit through synergistic interaction.

With respect to liver injury (Figure 15G–15U), the ABX+MOD group exhibited significantly elevated levels of ALT, AST, TG, TC, LDL, AKP, and TBA in both liver tissue and serum, accompanied by a marked reduction in HDL. Compared with their respective monotherapy counterparts, combination interventions (bacterial strain + NaB) demonstrated significantly greater efficacy in reducing hepatic and serum levels of TG, LDL, ALT, and AST (all $P < 0.05$). Moreover, the co-administration regimens involving ML, T23, and TF achieved significantly greater improvements in hepatic AKP activity and serum TBA concentrations than the corresponding single-strain treatments, underscoring an enhanced hepatoprotective and metabolic regulatory effect conferred by the addition of NaB.

Assessment of inflammatory cytokines (Figure 16A–16H) revealed that the ABX+MOD group exhibited significantly elevated levels of pro-inflammatory TNF-α, IL-6, and IL-1 in both liver tissue and serum, concomitant with a marked reduction in the anti-inflammatory cytokine IL-10. Across all five strains, combination therapy (probiotics strain + NaB) consistently achieved greater suppression of pro-inflammatory cytokines than monotherapy alone. Notably, the ML + NaB and MN + NaB co-administration groups significantly enhanced IL-10 expression in both hepatic tissue and serum relative to their respective single-strain interventions. These findings provide compelling evidence that the functional bacterial strains and NaB act synergistically to modulate the host

immune response, reinforcing an anti-inflammatory milieu that may underlie their combined therapeutic benefit in alcoholic liver disease.

Subsequently, with regard to ethanol-metabolizing capacity (Figure 16I–16P), the ABX+MOD group exhibited significantly reduced activities of ADH and ALDH in both liver tissue and serum. All combination regimens (bacterial strain + NaB) significantly restored hepatic ADH activity compared with their respective monotherapy groups. Notably, the ML + NaB and TF + NaB co-administration groups demonstrated significantly greater enhancement of serum ADH activity, as well as both hepatic and serum ALDH activity, relative to single-strain interventions alone. Furthermore, protein abundances of ADH and ALDH were markedly increased in the ML + NaB and TF + NaB groups compared with monotherapy, indicating that the synergistic interaction between these strains and NaB not only augments enzymatic activity but also upregulates enzyme expression. Collectively, these findings suggest that the combination of specific probiotic strains with NaB enhances host capacity for ethanol clearance through coordinated upregulation of both the expression and activity of key ethanol-metabolizing enzymes, thereby mitigating ethanol-induced hepatotoxicity.

Histopathological analysis of liver tissues further corroborated these biochemical and functional findings. H&E staining of liver sections (Figure 17A) revealed that mice in the ABX+MOD group exhibited extensive macro vesicular steatosis accompanied by mild inflammatory infiltration, severe disruption of hepatic architecture, and marked disorganization of lobular structure—hallmarks of classic alcohol-induced liver injury. Monotherapy with each candidate strain partially ameliorated hepatic steatosis to varying degrees, as evidenced by a noticeable reduction in lipid vacuoles and partial restoration of hepatocellular morphology and cord-like arrangement. Strikingly, combination therapy with NaB led to near-complete resolution of lipid droplets across all groups; residual steatosis was limited to sparse, small vacuoles in only a few hepatocytes, with overall cellular morphology closely resembling that of healthy controls. Among the combination regimens, ML + NaB, MN + NaB, and T23 + NaB demonstrated the most pronounced histological improvements, underscoring their superior efficacy in reversing alcohol-associated structural damage and restoring hepatic integrity.

H&E staining of colonic tissue (Figure 17B) showed that the ABX+CON group exhibited intact mucosal architecture, with well-organized villi, tightly aligned epithelial cells, and uniformly distributed goblet cells. In contrast, the ABX+MOD group displayed marked histopathological alterations: villi were shortened and partially fused, goblet cell numbers were reduced, epithelial cell alignment was disordered, and mild inflammatory infiltration was observed in the lamina propria—collectively indicative of intestinal mucosal injury. Monotherapy with individual bacterial strains partially restored villus architecture and length to varying degrees, enhanced epithelial integrity, and increased goblet cell density. Combination therapy with NaB further improved these parameters: villi exhibited greater height and structural regularity, epithelial continuity was markedly enhanced, and overall mucosal repair was substantially advanced. Notably, in the ML + NaB, TF + NaB, and T23 + NaB groups, colonic morphology closely resembled that of the control, suggesting a robust capacity of these combinations to restore intestinal mucosal integrity. Immunofluorescence analysis of tight junction proteins revealed significantly reduced expression of ZO-1 and occludin in the ABX+MOD group (Figure 18A-18C). Monotherapy consistently increased the expression of both proteins relative to the model group. Strikingly, co-administration with NaB further elevated ZO-1 and occludin levels, with several combination groups restoring expression to near-control values. These findings collectively demonstrate that probiotic–NaB co-intervention exerts a potent restorative effect on the intestinal epithelial barrier, reinforcing mucosal structure and tight junction integrity in the context of alcohol-induced gut injury.

Discussion

Probiotics defined as live microorganisms that confer health benefits to the host exert positive effects on host physiology through multiple mechanisms, including the modulation of gut microbial composition, enhancement of immune function, and facilitation of nutrient absorption[15]. Emerging evidence suggests their therapeutic potential in gastrointestinal disorders such as gastritis and colitis[16]. Furthermore, probiotics have been shown to protect against ALD via a multifaceted array of actions, including antioxidant activity, regulation of hepatic lipid metabolism, anti-inflammatory effects, restoration of intestinal barrier integrity, immunomodulation, and rebalancing of the gut microbiota[17-19]. However, to date, ethanol-metabolizing probiotic strains reported in the literature

have predominantly been isolated from fermented foods and beverages, such as baijiu (Chinese liquor), kimchi, and yak yogurt[20-22], with no documented isolates derived from human fecal samples. These findings inspired a novel hypothesis for our investigation: individuals who consume alcohol chronically yet remain free of liver injury may harbor gut-resident bacterial strains capable of metabolizing ethanol. Accordingly, we undertook the isolation and characterization of ethanol-metabolizing bacterial strains from the feces of such individuals.

Studies have reported distinct gut microbial profiles between healthy controls and individuals with heavy alcohol consumption who remained clinically asymptomatic[23]. In the latter group, increased abundances of potentially pathogenic taxa including *Enterobacteriaceae*, *Clostridia*, *Streptococcaceae*, and *Veillonellaceae* were observed. Moreover, when comparing these heavy-drinking healthy individuals with patients diagnosed with moderate-to-severe alcoholic hepatitis, the latter exhibited significantly reduced levels of SCFAs-producing families such as *Lachnospiraceae* and *Ruminococcaceae*. These findings suggest that even among individuals exposed to chronic alcohol intake, gut microbiota composition differs markedly between those who remain asymptomatic and those who develop ALD. Supporting this notion, animal studies have further demonstrated that alcohol-tolerant and alcohol-sensitive mice harbor significantly divergent gut microbial communities[24]. Specifically, alcohol-sensitive mice exhibited a marked reduction in *Bacteroidetes* abundance. Notably, fecal microbiota transplantation from alcohol-tolerant donors to alcohol-sensitive recipients substantially ameliorated hepatic injury and restored intestinal homeostasis. Inspired by these observations, we focused on healthy individuals with high-level alcohol tolerance who maintain hepatic and gastrointestinal health despite prolonged, heavy alcohol exposure, and hypothesized that their gut microbiota might harbor bacterial strains capable of tolerating and metabolizing ethanol. Guided by this premise, we successfully isolated multiple ethanol-metabolizing probiotic strains from their fecal samples.

Following alcohol ingestion, ethanol is primarily oxidized to acetaldehyde, a highly toxic intermediate by ADH, and subsequently converted to acetate by ALDH[25]. Central to this metabolic cascade is ALDH, given that acetaldehyde—a Group 1 human carcinogen—is implicated in the pathogenesis of hepatic, colorectal, and other malignancies[26]. Notably, *Lactobacillus plantarum*

has been shown to enhance both the activity and expression levels of ADH and ALDH, thereby directly engaging in ethanol metabolism and reducing systemic ethanol absorption[27,28]. Further evidence comes from a strain of *L. plantarum* (BGI-J9), isolated from traditional fermented yak yogurt in Inner Mongolia, which harbors a complete set of genes encoding enzymes involved in both ethanol and acetaldehyde metabolism and exhibits robust ethanol-degrading capacity[29]. Multiple subsequent studies have corroborated that putative probiotic strains carrying intact adh and aldh gene clusters demonstrate potent biodegradation capabilities against both ethanol and acetaldehyde[30-32]. In our study, pangenomic analysis, combined with phylogenetic reconstruction and ANI heatmaps, confirmed that all candidate isolates belong to the lactic acid bacteria (LAB) clade. Circular genome maps further revealed that each candidate strain possesses a comprehensive repertoire of genes encoding key enzymes in ethanol metabolism, including multiple subtypes of adh family genes and aldh homologs, collectively forming a putative two-step enzymatic pathway for efficient ethanol detoxification. This genomic architecture aligns closely with findings reported in prior investigations.

Studies have shown that NaB plays a pivotal role in modulating gut microbiota, restoring intestinal barrier integrity, and maintaining immune homeostasis[33-35]; our findings are consistent with these observations. Hu et al. demonstrated that NaB as a major source of SCFAs promotes the proliferation of beneficial bacteria such as *Lactobacillus* and *Bifidobacterium*, while suppressing the overgrowth of opportunistic pathogens including *Escherichia coli* and *Clostridioides difficile*[36], thereby effectively correcting microbial dysbiosis[37]. Preclinical evidence further indicates that NaB supplementation enhances α-diversity of the gut microbiota, particularly increasing the relative abundance of butyrate-producing bacteria, such as strains within the genus *Clostridium*[38]. In this study, we observed a significant reduction in microbial diversity in the MOD group, which was partially reversed by NaB intervention with restoration of microbial richness. Other studies have confirmed that probiotic strains including *Lactobacillus*, *Bifidobacterium*, and *Lactobacillus rhamnosus* effectively reshape the gut microbial community, preserve intestinal barrier function, mitigate inflammation, and enhance the activity of ADH and ALDH[39-42], collectively contributing to ALD improvement through multifaceted pathways. Guided by these findings, we co-cultured 14

ethanol-metabolizing bacterial isolates with NaB *in vitro*. Results demonstrated that NaB promoted the growth of five specific strains: ML, MN, T2, T23, and TF. To further dissect the individual effects of each strain and evaluate potential synergistic interactions with NaB, we conducted in vivo experiments. Our data revealed that both monotherapy with individual strains and combination therapy (strain + NaB) significantly improved hepatic and serum markers, including reductions in TG, LDL, ALT, and AST. Both regimens also markedly suppressed pro-inflammatory cytokines (TNF-α, IL-6, IL-1β) while elevating the anti-inflammatory cytokine IL-10. Moreover, they effectively restored ADH and ALDH enzymatic activities and increased their protein expression levels. Notably, the combination therapy consistently outperformed monotherapy across all assessed parameters, demonstrating superior efficacy in improving liver injury and ethanol metabolic capacity.

Conclusion

In this study, we successfully isolated and characterized probiotic strains with ethanol-metabolizing capacity from the fecal microbiota of healthy individuals with chronic alcohol tolerance. We subsequently undertook a comparative evaluation of monotherapy with the single strain versus combination therapy with NaB, thereby elucidating the mechanisms underlying the anti-ALD protective effects exerted by these ethanol-metabolizing probiotic strains both as monotherapy and in synergy with NaB (Figure 19). These findings provide a robust experimental basis for developing a novel composite microbial formulation that combines ethanol-metabolizing probiotic strains with NaB, offering a promising microbiota-targeted therapeutic strategy for the clinical management of ALD.

Materials and Methods

1. Participants

This study recruited healthy alcohol-tolerant individuals defined as those with long-term alcohol consumption but no evidence of liver injury from the outpatient clinic of the Department of Gastroenterology at the General Hospital of Ningxia Medical University. Eligible participants were

aged 40–80 years, had a history of alcohol consumption for ≥10 years, and reported average daily alcohol intake exceeding 40 g for men or 20 g for women. All participants had normal hepatic morphology and echogenicity on abdominal ultrasonography within the past six months and exhibited normal complete blood counts, coagulation profiles, and liver biochemistry. Individuals with viral hepatitis, autoimmune liver disease, drug-induced liver injury, or any other identifiable cause of liver dysfunction, as well as those with clinically significant comorbidities that could interfere with study participation or personal health, were excluded. The study protocol was approved by the Ethics Committee of Ningxia Medical University (Approval No.: 2020-053). The study was conducted in accordance with the Declaration of Helsinki. All participants provided written informed consent after being fully informed of the study procedures and voluntarily donated biological specimens for research purposes.

2. Isolation, identification, and evaluation of the biological characteristics of functional bacterial strains

2.1 Isolation of ethanol-metabolizing probiotic strains

Fresh fecal samples were collected from healthy alcohol-tolerant donors and immediately subjected to primary homogenisation in sterile saline under aseptic conditions. High-purity bacterial suspensions were then obtained through high-speed homogenisation followed by sequential filtration through membrane filters. The resulting suspension was serially diluted (from 10^{-1} to 10^{-8}) and plated onto multiple selective media including TPY, MRS, and BHI using the spread-plate technique. Plates were incubated under strict anaerobic conditions, and morphologically distinct single colonies were selected. Pure cultures were established through repeated streaking for isolation. These isolates were subsequently challenged in liquid media supplemented with increasing ethanol concentrations to assess alcohol tolerance. Strains capable of sustained growth in the presence of up to 15% (v/v) ethanol were identified as highly ethanol-tolerant and retained for further characterization[43].

2.2 Mass spectrometry for preliminary identification

The isolated bacterial strains were plated onto their respective optimal agar media at appropriate

concentrations and incubated at 37°C in an atmosphere containing 5–10% CO_2 for 48 hours. Individual colonies from each plate were then selected and subjected to preliminary species identification using the bioMérieux VITEK® MS microbial identification system. Each strain was analyzed in at least three biological replicates per plate to ensure reproducibility[44,45].

2.3 Ethanol degradation assay

Ethanol concentrations were measured using a portable alcohol meter manufactured by Xingweiqiang Co., Ltd. (Hebei, China), and the ethanol degradation rate was calculated based on the ethanol concentrations recorded at each time point.

2.4 Bile salt tolerance assay

Bacterial strains were anaerobically cultured in their respective liquid media for 48 h, and the cell density was adjusted to 1×10^9 CFU/mL. Equal volumes of bacterial suspension were then inoculated into pre-prepared liquid media supplemented with bile salts at final concentrations of 3% and 5% (v/v). Optical density at OD_{600} was measured using a microplate reader at 0, 2, 4, 6, and 8 hours post-inoculation to assess bacterial growth under bile salt stress[44,45].

2.5 Acid tolerance assay

Bacterial strains were anaerobically cultured in their respective liquid media for 48 hours, and the cell density was adjusted to 1×10^9 CFU/mL. Equal volumes of bacterial suspension were then inoculated into pre-prepared liquid media acidified with hydrochloric acid, with pH adjusted to 2.0 and 3.0 using a calibrated pH meter. Optical density at OD_{600} was measured using a microplate reader at 0, 2, 4, and 6 hours post-inoculation to evaluate bacterial viability under acidic conditions[44,45].

2.6 Gram staining

Smears prepared from single colonies were air-dried, heat-fixed, and subjected to Gram staining (crystal violet, iodine mordant, ethanol decolourisation, and safranin counterstain). Microscopy revealed Gram-positive bacteria as blue–purple and Gram-negative bacteria as red[46].

2.7 Identification of ethanol-metabolizing probiotic strains

We performed whole-genome shotgun metagenomic sequencing on the 14 isolated and identified bacterial strains. Genomic DNA was fragmented to an average insert size of approximately 400 bp using the Covaris M220 ultrasonicator. Paired-end sequencing libraries were then constructed using the NEXTFLEX® Rapid DNA-Seq Kit (Bioo Scientific, Austin, Texas, USA). Sequencing was carried out on a NovaSeq 6000 platform (Illumina, San Diego, California, USA) at Mejo Biopharma Co., Ltd. (Shanghai, China). Raw sequencing data were processed on the Majorbio Cloud Platform. Briefly, adapter sequences and low-quality reads were removed using *fastp*, with stringent filtering criteria applied: reads shorter than 50 bp, those with a Phred quality score below 20, or those containing ambiguous (N) bases were excluded from downstream analyses.

Although pure bacterial isolates (single-colony cultures) were successfully obtained from the gut microbiota of alcohol-tolerant individuals in this study, metagenomic DNA—rather than isolate genomic DNA—was inadvertently submitted for sequencing. Subsequent analyses were therefore based on contigs assembled from metagenomic reads. These contigs were uploaded to the Type (Strain) Genome Server (TYGS; https://tygs.dsmz.de) to infer phylogenetic relationships, and the resulting phylogenetic tree was visualized and refined using the iTOL platform. Closely related reference strains were identified based on phylogenetic clustering, and their complete genome sequences were retrieved from the NCBI Assembly database. Average nucleotide identity (ANI) values between candidate contigs and reference genomes were computed using the ANIfast tool under the Ubuntu operating system, and the resulting similarity matrix was visualized as a heatmap in R. Genome circular maps of the candidate strains—reconstructed from metagenome-assembled contigs—were generated using the online ProkSee platform (https://proksee.ca). These maps were annotated to display key genomic features, including GC content, coding sequences (CDS), RNA genes, and core genes involved in ethanol metabolism. Functional annotations based on COG, KEGG, and CAZy databases were performed using output files from the Majorbio Cloud Platform and subsequently visualized with R[29,47].

2.8 Growth kinetics

The 14 candidate bacterial strains isolated from healthy alcohol-tolerant individuals were individually inoculated into TPY or MRS liquid media, with the initial cell density adjusted to 1×10^9 CFU/mL. Four experimental conditions were established for each strain: (1) bacteria alone (control), (2) bacteria + NaB, (3) bacteria + ethanol, and (4) bacteria + ethanol + NaB. Equal volumes of bacterial suspension were added to pre-prepared culture media supplemented with ethanol, NaB, or neither, as appropriate. In ethanol-containing groups, the final ethanol concentration was adjusted to 15% (v/v). Each condition was tested in at least six replicate wells. OD_{600} was measured at defined time points using a microplate reader, and growth curves were generated by plotting OD values against time[48].

3. *In Vivo* intervention study with ethanol-metabolizing probiotic strains

We evaluated the five candidate functional bacterial strains—identified in vitro as exhibiting synergistic effects with NaB. Each strain was separately cultured anaerobically in its respective liquid medium for 48 hours, and the resulting bacterial suspension was adjusted to a concentration of 1×10^9 CFU/mL. Mice in the monotherapy groups received daily oral gavage of 1×10^8 CFU of the respective bacterial strain. In the combination therapy groups, mice received the same bacterial dose (1×10^8 CFU) co-administered with sodium butyrate at a dose of 0.6 g/kg body weight. Both interventions were administered once daily for six consecutive weeks.

4. Probiotic strains with ethanol-metabolizing capacity

The strains [ML, MN, T2, T23, and TF] used in this study were isolated from the fecal samples of individuals with chronic alcohol consumption but without liver injury. These strains have been deposited in the China Center for Type Culture Collection (CCTCC) under the accession numbers CCTCC M 2026437, CCTCC M 2026440, CCTCC M 2026438, CCTCC M 2026439, and CCTCC M 2026436, respectively.

5. Animals

All animal experimental procedures were approved by the Ethics Committee of Ningxia Medical University (Approval No. 2020-053) and conducted in strict accordance with the *Regulations on the Management of Laboratory Animals* of Ningxia Medical University. Female, 8-week-old, specific

pathogen–free (SPF) C57BL/6J mice were sourced from Vital River Laboratory Animal Technology Co., Ltd. (Beijing, China). Animals were housed at the Experimental Animal Center of Ningxia Medical University (Yinchuan, China) under controlled environmental conditions (temperature: 22 ± 2°C; humidity: 45 ± 5%; 12-hour light–dark cycle) and had ad libitum access to standard chow and water throughout the study. Following antibiotic (ABX) treatment, mice were allocated into the following experimental groups (n=8 per group): Control group, ABX-treated normal control (ABX+CON) and ABX-treated alcoholic liver disease model (ABX+MOD); Treatment groups including ABX+MOD mice further received ML (ABX+MOD+ML), MN (ABX+MOD+MN), T2 (ABX+MOD+T2), T23 (ABX+MOD+T23), or TF (ABX+MOD+TF); Combination Therapy group, ABX+MOD mice received the aforementioned treatments combined with NaB (i.e., ABX+MOD+ML+NaB, ABX+MOD+MN+NaB, ABX+MOD+T2+NaB, ABX+MOD+T23+NaB, and ABX+MOD+TF+NaB).

Acclimatization Protocol: The control group (ABX+CON) received the Lieber-DeCarli control liquid diet exclusively for six consecutive days, with a daily provision of 30 mL per mouse. The alcohol-exposed groups (including ABX+MOD and all associated treatment arms) underwent a 6-day graded ethanol exposure regimen to induce tolerance. This involved a stepwise increase in the proportion of alcohol-containing diet mixed with the control diet: a 1:2 ratio for the initial 2 days, followed by a 1:1 ratio for the subsequent 2 days, and concluding with a 2:1 ratio for the final 2 days. The total daily volume was maintained at 30 mL per mouse throughout this period.

Experimental Intervention: Following the acclimatization period, the modeling phase was initiated. The ABX+CON group continued to receive the Lieber-DeCarli control liquid diet, while all alcohol-exposed groups (including ABX+MOD and its derivative treatment arms) were switched to the Lieber-DeCarli alcohol liquid diet containing approximately 1.2 g of ethanol per 30 mL (derived from 95% anhydrous ethanol). Both diets were provided at a fixed daily volume of 30 mL per mouse. Concurrently, mice in the monotherapy groups received daily oral gavage of 1×10^8 CFU of their respective bacterial strain. Mice in the combination therapy groups were administered the same bacterial dose (1×10^8 CFU) co-formulated with sodium butyrate at 0.6 g/kg of body weight. The ABX+CON and ABX+MOD groups received an equivalent volume of sterile normal

saline via gavage. These interventions were administered once daily for a consecutive period of six weeks.

6. Model induction and NaB administration

To establish a murine model of ALD, female C57BL/6J mice were randomly allocated into four groups (n = 8 per group): a normal control group (CON), an ALD model group (MOD), a sNaB control group (CON+NaB), and an alcohol plus NaB group (MOD+NaB). Mice were fed the Lieber–DeCarli ethanol liquid diet (Catalog No. TP4030M3; Trophic Diet Technology Co., Ltd., Nantong, China) for six weeks. This diet provided 28% of total calories from ethanol, with the remaining energy derived from 18% protein, 19% carbohydrate, and 35% fat. Control animals received an isocaloric Lieber–DeCarli control liquid diet (Catalog No. TP4030M3C), in which ethanol-derived calories were replaced by maltodextrin. NaB (Sigma-Aldrich, St. Louis, MO, USA) was administered daily via oral gavage at a dose of 0.6 g per kg body weight. Mice in the control and model groups received an equivalent volume of sterile saline by gavage. At the end of the intervention period, fresh fecal samples were collected from all groups and immediately stored at –80°C for subsequent microbiome sequencing analyses. Mice were deeply anesthetized by intraperitoneal injection of sodium pentobarbital (80 mg/kg body weight). After confirming the loss of pedal reflex, blood was collected via retro-orbital (orbital sinus) bleeding. Mice were then euthanized by cervical dislocation. All efforts were made to minimize suffering. Liver and colonic tissues were harvested for biochemical, histological, and molecular assessments.

7. Biochemical parameter analysis

Peripheral blood samples were centrifuged at 500 × g for 15 minutes, and the supernatant plasma was collected. Liver tissues were homogenized in ice-cold phosphate-buffered saline (PBS) containing protease inhibitors at a ratio of 0.1 g tissue per mL, followed by centrifugation at 3,000 × g for 15 minutes; the resulting supernatants were used for biochemical analyses. Commercial assay kits for ALT, AST, TC, TG, HDL, LDL, AKP, and TBA were obtained from Nanjing Jiancheng Bioengineering Institute (Nanjing, China).

8. Enzyme-linked immunosorbent assay (ELISA)

Plasma and liver tissue supernatants were prepared as described in Section 7. Commercial ELISA kits for TNF-α, IL-1β, IL-6, and IL-10 were obtained from Wuhan Sanying Biotechnology Co., Ltd. (Wuhan, China). Assay kits for ADH and ALDH activities were sourced from Suzhou Keming Biological Technology Co., Ltd. (Suzhou, China), while kits for quantifying ADH and ALDH protein levels were purchased from Shanghai Jianglai Biotechnology Co., Ltd. (Shanghai, China). All assays were performed strictly in accordance with the manufacturers' instructions.

9. Plasma endotoxin assay

Plasma endotoxin levels in mice were quantified using the chromogenic limulus amebocyte lysate (LAL) assay according to the manufacturer's instructions (Xiamen Limulus Reagent Bio-Tech Co., Ltd., Xiamen, China). Briefly, 100 μL of endotoxin-free water, standard solutions, or plasma samples were added to individual reaction tubes, followed by the addition of 100 μL of LAL reagent. The mixtures were incubated at 37°C for 30 minutes in the dark. Subsequently, 100 μL of chromogenic substrate solution was added to each tube, and the reaction was continued at 37°C for 6 minutes under light-protected conditions. The reaction was then terminated by adding 100 μL of azo-coupling reagent, followed by gentle mixing and a 5-minute incubation at room temperature in the dark. Absorbance was measured at 545 nm using a microplate reader, and LPS concentrations were calculated based on the optical density (OD) values relative to the standard curve.

10. Hematoxylin and Eosin (H&E) staining

Liver and colonic tissues were harvested from mice, fixed in 4% paraformaldehyde, processed through standard histological protocols, and embedded in paraffin. Serial sections (5 μm thick) were cut and stained with H&E for histopathological evaluation.

11. Immunofluorescence staining

Colonic tissues were fixed, embedded, and sectioned as described in Section 10. Immunofluorescence staining was performed using primary antibodies against occludin (Catalog No. CMA9060) and ZO-1 (Catalog No. CMA9003), both sourced from Hangzhou Kanghexin Biotechnology Co., Ltd. (Hangzhou, China). Stained sections were examined under an Olympus fluorescence microscope, and high-resolution whole-slide images were acquired using the

Pannoramic Scanner imaging system. Quantitative analysis of fluorescence intensity and distribution was carried out using ImageJ software (National Institutes of Health, USA).

12. 16S rRNA gene sequencing

Genomic DNA was extracted from each sample, and its purity and concentration were assessed by agarose gel electrophoresis, followed by dilution to a final concentration of 1 ng/μL. Using the diluted genomic DNA as template, the V3–V4 hypervariable regions of the 16S rRNA gene were amplified with barcoded primers and Phusion® High-Fidelity PCR Master Mix with GC Buffer (New England Biolabs). High-efficiency, high-fidelity PCR was performed to ensure both amplification yield and sequence accuracy. Equal amounts of PCR products, normalized by concentration, were pooled, thoroughly mixed, and the target amplicons were purified using the QIAquick Gel Extraction Kit (Qiagen). SMRTbell libraries were constructed, and insert sizes were validated using the Agilent 2100 Bioanalyzer prior to sequencing on the PacBio platform[49]. Raw PacBio reads were demultiplexed using the *lima* software based on barcode sequences. Circular Consensus Sequencing (CCS) was performed via SMRT Link v7.0 to generate high-quality consensus reads, which were exported in both FASTQ and FASTA formats. Subsequently, reads underwent stringent quality filtering: primers were trimmed using *cutadapt*, and sequences containing homopolymer runs longer than eight identical nucleotides were removed, yielding high-quality "Clean Reads"[50]. All Clean Reads across samples were clustered into operational taxonomic units (OTUs) at a default 97% sequence identity threshold using the UPARSE pipeline (UPARSE v7.0.1001; http://drive5.com/uparse/). Taxonomic annotation was performed using the Mothur-compatible workflow against the SILVA SSU rRNA reference database (https://www.arb-silva.de/) to assign taxonomic identities and quantify community composition across all taxonomic levels. Prior to diversity analyses, data were rarefied to the depth of the sample with the highest sequencing coverage to ensure comparability. Alpha and beta diversity metrics were computed accordingly[51]. Alpha diversity indices (e.g., Shannon, Simpson, Chao1) were calculated using QIIME (v1.9.1), while rarefaction curves, rank-abundance curves, and species accumulation curves were generated in R (v2.15.3). For intergroup comparisons of alpha diversity, parametric (Student's *t*-test) or non-parametric (Wilcoxon rank-sum test) methods were applied for two-group

comparisons; for multi-group analyses, Tukey's honest significant difference (HSD) test and pairwise Wilcoxon tests with the *agricolae* package were employed. Beta diversity was assessed via principal coordinates analysis (PCoA), implemented in R using the *WGCNA*, *stats*, and *ggplot2* packages, and non-metric multidimensional scaling (NMDS) was performed using the *vegan* package in R. Differential abundance analysis was conducted using LEfSe (Linear Discriminant Analysis Effect Size), with a default LDA score threshold of 3. Additionally, Metastats analysis was performed in R across all taxonomic levels using permutation tests to obtain *p*-values, which were subsequently adjusted for multiple testing using the Benjamini–Hochberg false discovery rate (FDR) method to yield *q*-values[52]. To explore microbial co-occurrence patterns, Spearman and Pearson correlation coefficients were calculated between all genus-level taxa based on relative abundances. A correlation matrix was constructed and filtered under the following criteria: (a) only correlations with absolute coefficient > 0.6 were retained; (b) self-loops (i.e., correlations of a tax on with itself) were excluded; and (c) edges involving taxa with mean relative abundance < 0.001% were removed. The resulting network was visualized using Gephi (v0.10.1), with genera as nodes and significant correlations as edges. Functional potential of the microbial communities was inferred using both Tax4Fun and PICRUSt2 to predict KEGG pathway abundances[53], and results were visualized using R.

13.ABX treatment

Each mouse received daily oral gavage of 100 μL of a solution containing ampicillin (5 mg/mL), neomycin sulfate (5 mg/mL), metronidazole (5 mg/mL), and vancomycin (2.5 mg/mL)—all sourced from Macklin Biochemical Co., Ltd. (Shanghai, China)—for a total duration of one week.

14. Statistical analysis

All experimental data were analyzed using GraphPad Prism version 9.0 (GraphPad Software, San Diego, CA, USA), OriginPro 2025b (OriginLab Corporation, Northampton, MA, USA), and R Studio (version 2025.09.2+418; R Foundation for Statistical Computing, Vienna, Austria). Data are presented as mean ± standard deviation (SD). For comparisons across multiple groups, two-way analysis of variance (two-way ANOVA) was employed, followed by appropriate post hoc tests.

Comparisons between two groups were performed using a two-tailed Student's *t*-test, assuming normal distribution. Correlation analyses were conducted using Spearman's rank correlation coefficient. A *P* value of less than 0.05 was considered statistically significant.

Acknowledgments

We especially thank Ningxia Key Laboratory of Infection and Immunity, School of Basic Medical Sciences, Ningxia Medical University, for providing the research platform essential to this work. We also extend our sincere appreciation to the Microbiome Unit of the Medical Research Center at the General Hospital of Ningxia Medical University for supplying critical instrumentation including anaerobic chambers, mass spectrometry systems, and microplate readers that enabled the successful isolation, purification, and identification of bacterial strains in this project. Finally, we are deeply grateful to all members of our lab "Family 120" for their steadfast support and contributions, which were instrumental to the progress and completion of this study.

Funding

This work was supported by National Natural Science Foundation of China (Grant No. 82160122), the Program of Ningxia Science and Technology Leading Talent, China (Grant No. 2023GKLRLX19, 2023GKLRLX17), , the Key Research and Development Program of Ningxia, China (Grant No. 2023BEG02011), the Ningxia Gut Homeostasis and Chronic Disease Prevention and Treatment Scientific and Technological Innovation Team, China (Grant No. 2022BSB03112) and Ningxia Natural Science Foundation, China (Grant No. 2023AAC03535).

Author contributions

H W, S Y and X Z conceived and designed the study. F L and J L jointly performed animal husbandry, bacterial strain isolation, purification, and identification, conducted experiments, and carried out data analysis; F L drafted the manuscript. Y K assisted with animal husbandry, and Y L contributed to in vivo experimental procedures. T M was responsible for tissue embedding, sectioning, and

histological staining. J M and J L assisted with animal tissue harvesting. P Y, S L and L Z supported the dissection and preservation of animal tissues. L Z, H W and S Y provided the fundings. All authors have read and approved the final version of the manuscript.

Limitations

The precise molecular mechanisms by which NaB enhances the growth of specific bacterial strains—such as whether this effect is mediated through metabolic pathways including the pentose phosphate pathway, glycolysis, or branched-chain amino acid biosynthesis—remain to be fully elucidated. Moreover, the current cohort of healthy alcohol-tolerant individuals is limited in size; future studies should enrol larger, well-characterised cohorts to enable the discovery of additional functionally relevant microbial taxa. Furthermore, for those strains that demonstrate marked efficacy in combination therapy with NaB, high-quality whole-genome sequencing is essential to delineate the genetic determinants underpinning their beneficial phenotypes.

Data availability

The datasets presented in-this-study can be found in online repositories. The names of the repository/repositories and accession number(s)can be found below: NCBI, accession number PRJNA1424367.

Conflict of interest

The authors declare no competing interests.

Declarations

Ethics approval and consent to participate

All experimental protocols involving human participants were approved by the Ethics Committee of Ningxia Medical University (Approval No.: 2020-053). The study was performed in accordance with the Declaration of Helsinki. Written informed consent was obtained from all individual participants included in the study.

All animal experimental procedures were approved by the Ethics Committee of Ningxia Medical University (Approval No.: 2020-053) and complied with the ARRIVE guidelines. Mice were deeply anesthetized via intraperitoneal injection of sodium pentobarbital (80 mg/kg body weight). After confirmation of deep anesthesia by loss of pedal reflex, blood was collected via retro-orbital bleeding, followed by euthanasia by cervical dislocation. All efforts were made to minimize animal suffering.

Consent for publication

Not applicable. This manuscript does not contain any individual person's data in any form (including images, videos, or clinical details that could compromise anonymity).

References

[1] HE Q, YANG C, KANG X, et al. Intake of Bifidobacterium lactis Probio-M8 fermented milk protects against alcoholic liver disease [J]. Journal of dairy science, 2022, 105(4): 2908-21.

[2] ÇOLAKOĞLU M, XUE J, TRAJKOVSKI M. Bacteriophage Prevents Alcoholic Liver Disease [J]. Cell, 2020, 180(2): 218-20.

[3] NARRO G E C, DíAZ L A, ORTEGA E K, et al. Alcohol-related liver disease: A global perspective [J]. Annals of hepatology, 2024, 29(5): 101499.

[4] ZHAI M, LONG J, LIU S, et al. The burden of liver cirrhosis and underlying etiologies: results from the global burden of disease study 2017 [J]. Aging, 2021, 13(1): 279-300.

[5] ÅBERG F, JIANG Z G, CORTEZ-PINTO H, et al. Alcohol-associated liver disease-Global epidemiology [J]. Hepatology (Baltimore, Md), 2024, 80(6): 1307-22.

[6] FENG S, ROLL G R, ROUHANI F J, et al. The future of liver transplantation [J]. Hepatology (Baltimore, Md), 2024, 80(3): 674-97.

[7] GHELICHI-GHOJOGH M, RAJABI A, MOHAMMADIZADEH F, et al. Survival Rate of Liver Transplantation in Asia: A Systematic Review and Meta-Analysis [J]. Iranian journal of public health, 2022, 51(10): 2207-20.

[8] JANDHYALA S M, TALUKDAR R, SUBRAMANYAM C, et al. Role of the normal gut microbiota [J]. World journal of gastroenterology, 2015, 21(29): 8787-803.

[9] KOURKOUMPETIS T, SOOD G. Pathogenesis of Alcoholic Liver Disease: An Update [J]. Clinics in liver disease, 2019, 23(1): 71-80.

[10] GAN Y, TONG J, ZHOU X, et al. Hepatoprotective Effect of Lactobacillus plantarum HFY09 on Ethanol-Induced Liver Injury in Mice [J]. Frontiers in nutrition, 2021, 8: 684588.

[11] LI H, SHI J, ZHAO L, et al. Lactobacillus plantarum KLDS1.0344 and Lactobacillus acidophilus KLDS1.0901 Mixture Prevents Chronic Alcoholic Liver Injury in Mice by Protecting the Intestinal Barrier and Regulating Gut Microbiota and Liver-Related Pathways [J]. Journal of agricultural and food chemistry, 2021, 69(1): 183-97.

[12] AHMADI BADI S, TAVAKOLI AVAL H, MORADI H R, et al. Comparative study of liver

injury protection by Akkermansia muciniphila and Faecalibacterium prausnitzii interventions in live and cell-free supernatant forms via targeting the hepcidin - ferroportin axis in mice with CCl_4-induced liver fibrosis [J]. Gut pathogens, 2025, 17(1): 54.

[13] ZHANG L, MA Z, ZHANG X, et al. Butyrate alleviates alcoholic liver disease-associated inflammation through macrophage regulation and polarization via the HDAC1/miR-155 axis [J]. International immunopharmacology, 2024, 131: 111852.

[14] WEI H, YU C, ZHANG C, et al. Butyrate ameliorates chronic alcoholic central nervous damage by suppressing microglia-mediated neuroinflammation and modulating the microbiome-gut-brain axis [J]. Biomedicine & pharmacotherapy = Biomedecine & pharmacotherapie, 2023, 160: 114308.

[15] HSIEH P S, CHEN C W, KUO Y W, et al. Lactobacillus spp. reduces ethanol-induced liver oxidative stress and inflammation in a mouse model of alcoholic steatohepatitis [J]. Experimental and therapeutic medicine, 2021, 21(3): 188.

[16] STAVROPOULOU E, BEZIRTZOGLOU E. Probiotics in Medicine: A Long Debate [J]. Frontiers in immunology, 2020, 11: 2192.

[17] LI X, LIU Y, GUO X, et al. Effect of Lactobacillus casei on lipid metabolism and intestinal microflora in patients with alcoholic liver injury [J]. European journal of clinical nutrition, 2021, 75(8): 1227-36.

[18] VATSALYA V. Novel Biomarker for the Diagnosis and Prognosis of Acute Alcoholic Hepatitis [J]. Clinical & experimental pharmacology, 2020, 10(4).

[19] LIU Q, YU Z, TIAN F, et al. Surface components and metabolites of probiotics for regulation of intestinal epithelial barrier [J]. Microbial cell factories, 2020, 19(1): 23.

[20] WANG J, XU Q, LU C, et al. Probiotics isolated from the fermented grains of Chinese baijiu alleviate alcohol-induced liver injury by regulating alcohol metabolism and the gut microbiota in mice [J]. Food & function, 2025, 16(6): 2545-63.

[21] ZHANG J P, LI M L, REN D L, et al. High-throughput screening of probiotics in fermented foods and their potential application in alleviating alcohol-induced damage [J]. Food & function, 2025, 16(6): 2564-76.

[22] YI R, TAN F, LIAO W, et al. Isolation and Identification of Lactobacillus plantarum HFY05 from Natural Fermented Yak Yogurt and Its Effect on Alcoholic Liver Injury in Mice [J]. Microorganisms, 2019, 7(11).

[23] SMIRNOVA E, PURI P, MUTHIAH M D, et al. Fecal Microbiome Distinguishes Alcohol Consumption From Alcoholic Hepatitis But Does Not Discriminate Disease Severity [J]. Hepatology (Baltimore, Md), 2020, 72(1): 271-86.

[24] FERRERE G, WRZOSEK L, CAILLEUX F, et al. Fecal microbiota manipulation prevents dysbiosis and alcohol-induced liver injury in mice [J]. Journal of hepatology, 2017, 66(4): 806-15.

[25] KONG E Q Z, SUBRAMANIYAN V, LUBAU N S A. Uncovering the impact of alcohol on internal organs and reproductive health: Exploring TLR4/NF-kB and CYP2E1/ROS/Nrf2 pathways [J]. Animal models and experimental medicine, 2024, 7(4): 444-59.

[26] BROOKS P J, ZAKHARI S. Acetaldehyde and the genome: beyond nuclear DNA adducts and carcinogenesis [J]. Environmental and molecular mutagenesis, 2014, 55(2): 77-91.

[27] ZHANG L, ZHANG Y, LIU S, et al. Degradation effects and mechanisms of

Limosilactobacillus fermentum on ethanol [J]. Food & function, 2024, 15(20): 10283-99.
[28] WANG Z, HE J-J, LIU X-X, et al. High-level expression of an acetaldehyde dehydrogenase from Lactiplantibacillus plantarum and preliminary evaluation of its potential as a functional food additive [J]. 2023, 63: 1-9.
[29] FAN Y, MA Z, WEI B, et al. Revealing the potent probiotic properties and alcohol degradation capabilities of Lactiplantibacillus plantarum BGI-J9 by combining complete genomic and phenotypic analysis [J]. Frontiers in microbiology, 2025, 16: 1664033.
[30] LIU H, WANG J, XU Q, et al. Biodegradation of Both Ethanol and Acetaldehyde by Acetobacter ghanensis JN01 [J]. 2025, 15(8): 756.
[31] KANG S, LONG J, PARK M S, et al. Investigating human-derived lactic acid bacteria for alcohol resistance [J]. Microbial cell factories, 2024, 23(1): 118.
[32] GWAK J H, CHOI Y J, AYUB H, et al. Comprehensive genomic and functional analysis of Leuconostoc lactic acid bacteria in alcohol and acetaldehyde metabolism [J]. Journal of microbiology (Seoul, Korea), 2025, 63(2): e2410026.
[33] ZHOU D, PAN Q, XIN F Z, et al. Sodium butyrate attenuates high-fat diet-induced steatohepatitis in mice by improving gut microbiota and gastrointestinal barrier [J]. World journal of gastroenterology, 2017, 23(1): 60-75.
[34] BAO T, HE F, ZHANG X, et al. Inulin Exerts Beneficial Effects on Non-Alcoholic Fatty Liver Disease via Modulating gut Microbiome and Suppressing the Lipopolysaccharide-Toll-Like Receptor 4-Mψ-Nuclear Factor-κB-Nod-Like Receptor Protein 3 Pathway via gut-Liver Axis in Mice [J]. Frontiers in pharmacology, 2020, 11: 558525.
[35] LI G, LIN J, ZHANG C, et al. Microbiota metabolite butyrate constrains neutrophil functions and ameliorates mucosal inflammation in inflammatory bowel disease [J]. Gut microbes, 2021, 13(1): 1968257.
[36] XIAOYI H, HAIPENG W, JIANJUN Y, et al. Research progress on relationship between γ-aminobutyric acid system disorder and neurodegenerative diseases [J]. Journal of Clinical Anesthesiology, 2025, 41(1): 83-8. (in Chinese)
[37] QI S, YUNTIAN L, YANG Y, et al. Research progress on mechanism and clinical application of sodium butyrate in modulating the gut microbiota-metabolism-immunity axis in the treatment of acute pancreatitis [J]. Shandong Medical Journal, 2025, 65(11): 122-6. (in Chinese)
[38] LIU Y, CHEN Z, DAI J, et al. Sodium butyrate supplementation in high-soybean meal diets for turbot (Scophthalmus maximus L.): Effects on inflammatory status, mucosal barriers and microbiota in the intestine [J]. Fish & shellfish immunology, 2019, 88: 65-75.
[39] KAYAMA H, OKUMURA R, TAKEDA K. Interaction Between the Microbiota, Epithelia, and Immune Cells in the Intestine [J]. Annual review of immunology, 2020, 38: 23-48.
[40] MA L, NI Y, WANG Z, et al. Spermidine improves gut barrier integrity and gut microbiota function in diet-induced obese mice [J]. Gut microbes, 2020, 12(1): 1-19.
[41] CHOPYK D M, GRAKOUI A. Contribution of the Intestinal Microbiome and Gut Barrier to Hepatic Disorders [J]. Gastroenterology, 2020, 159(3): 849-63.
[42] JUNG S J, HWANG J H, PARK E O, et al. Regulation of Alcohol and Acetaldehyde Metabolism by a Mixture of Lactobacillus and Bifidobacterium Species in Human [J]. Nutrients, 2021, 13(6).
[43] SONG M, YUN B, MOON J H, et al. Characterization of Selected Lactobacillus Strains for

Use as Probiotics [J]. Korean journal for food science of animal resources, 2015, 35(4): 551-6.
[44] YUN M, JO H E, KIM N, et al. Oral Administration of Alcohol-Tolerant Lactic Acid Bacteria Alleviates Blood Alcohol Concentration and Ethanol-Induced Liver Damage in Rodents [J]. Journal of microbiology and biotechnology, 2024, 34(4): 838-45.
[45] REN J. Preparation of apple juice fermented with alcohol degrading function probiotics and its functional evaluation [J]. Dissertation Submitted to Northwest A&F Universityin Partial Fulfillment of the Requirements for the Degree of Master of Biology and Medicine, 2024. (in Chinese)
[46] JIANG Y. Evaluation of the Probiotic Properties of Endogenous Lactic Acid Bacteria in Honey Bees and Their Potential for Controlling American Foulbrood [J]. Yangzhou University in partial fulfillment of the requirements for the degree of Master of Engineering, 2025. (in Chinese)
[47] REN Y, YU G, SHI C, et al. Majorbio Cloud: A one-stop, comprehensive bioinformatic platform for multiomics analyses [J]. iMeta, 2022, 1(2): e12.
[48] JIN H. Study on Yeast Screening of Kiwifruit Wine and Optimization of Its Fermentation Conditions for Compound Barm [J]. Nanyang Normal University for Master Degree, 2022. (in Chinese)
[49] LI M, YU L, ZHAI Q, et al. Ganoderma applanatum polysaccharides and ethanol extracts promote the recovery of colitis through intestinal barrier protection and gut microbiota modulations [J]. Food & function, 2022, 13(2): 688-701.
[50] BOLYEN E, RIDEOUT J R, DILLON M R, et al. Reproducible, interactive, scalable and extensible microbiome data science using QIIME 2 [J]. Nature biotechnology, 2019, 37(8): 852-7.
[51] QUAST C, PRUESSE E, YILMAZ P, et al. The SILVA ribosomal RNA gene database project: improved data processing and web-based tools [J]. Nucleic acids research, 2013, 41(Database issue): D590-6.
[52] PARKS D H, TYSON G W, HUGENHOLTZ P, et al. STAMP: statistical analysis of taxonomic and functional profiles [J]. Bioinformatics (Oxford, England), 2014, 30(21): 3123-4.
[53] DOUGLAS G M, MAFFEI V, ZANEVELD J, et al. PICRUSt2: An improved and customizable approach for metagenome inference. bioRxiv: 672295 [J]. 2020.

Figure Legends

Figure 1. Isolation and functional characterization of ethanol-metabolizing gut bacteria from alcohol-tolerant individuals. Fecal samples were obtained from healthy individuals with a history of chronic alcohol consumption but no clinical evidence of liver injury. Subsequently, a comprehensive and systematic workflow was implemented for the isolation, identification, and functional validation of candidate bacterial strains.

Figure 2 Time-course analysis of ethanol degradation rate over 48 hours for 91 purified bacterial isolates. To evaluate the ethanol-degrading capacity of the candidate strains, we conducted a 48-hour kinetic monitoring assay. Twenty isolates (MB, MD, ME, MF, ML, MN, M1C, M2, M8, M15, M16, M34, M44, M46, TF, T2, T11, T13, T21, and T23) demonstrated rapid ethanol metabolism, achieving a degradation rate exceeding 10% at the 48-hour time point.

Figure 3-1. Taxonomic identification, and genomic characterization of ethanol-metabolizing bacterial strains from healthy alcohol-tolerant individuals. (A) Bile salt tolerance assay under 3% and 5% bile salt concentrations at four time points (2, 4, 6, and 8 h). **(B)** Acid tolerance assay under pH 2.0 and pH 3.0 conditions at three time points (2, 4, and 6 h). **(C)** Phylogenetic tree constructed from high-quality draft genomes assembled from metagenomic sequencing data of pure cultures, showing evolutionary relationships among the final 14 candidate isolates and reference type strains. **(D)** Average nucleotide identity (ANI) heatmap comparing candidate draft genomes with closely related reference genomes. **(E)** Circular genome maps of all 14 candidate draft genomes, illustrating chromosomal architecture and distribution of ethanol-metabolizing genes. Alcohol dehydrogenase (adhA/C/E/1–3) and aldehyde dehydrogenase (aldA/C/E/1) genes are highlighted in red in the outermost ring. Genomic analyses were performed on DNA extracted from pure cultures subjected to metagenomic sequencing.

Figure 3-2. In vitro functional annotation of candidate strains. (F) Clusters of Orthologous Groups (COG) classification: **(Ⅰ)** Bar plot showing the number of genes assigned to four advanced functional categories, **(Ⅱ)** Enrichment of metabolism-related COG subcategories, **(Ⅲ)** Heatmap of COG functional class distribution across all strains, with gene counts normalized by total coding sequence length. **(G)** KEGG pathway enrichment analysis: **(I)** Bar plot showing gene counts in the top 15 KEGG level 2 categories across all strains, **(II)** Bar plot showing gene counts in the top 15 metabolism-related KEGG level 3 categories. **(H)** Carbohydrate-Active enZymes (CAZy) profiling: **(I)** Heatmap of the top 20 most abundant CAZy families across all strains, **(II)** Bar plot showing gene counts for alcohol-related CAZy families. **(I)** Gram staining. Genomic analyses were performed on DNA extracted from pure cultures subjected to metagenomic sequencing.

Figure 4. Growth kinetics under ethanol-free or 15% ethanol conditions with or without NaB. To characterize the growth dynamics of ethanol-metabolizing probiotic candidates and their potential synergy with NaB, we evaluated strain proliferation under basal and ethanol-stressed conditions, both in the presence and absence of NaB. In the absence of ethanol, NaB significantly promoted the growth of strains ML, MN, T2, T23, and TF. Furthermore, upon exposure to a 15% (v/v) ethanol challenge, the co-administration of NaB significantly attenuated the ethanol-induced growth inhibition in these specific strains.

Figure 5. Ethanol-metabolizing lactobacilli isolated from alcohol-tolerant individuals protect against alcoholic liver injury in microbiota-depleted mice. (A) Experimental design and animal

groups (n = 8 per group). **(B)** Body weight changes over time. **(C)** Food intake **(D)** Blood glucose **(E)** Liver weight **(F)** Liver index **(G)** Liver ALT. **(H)** Liver AST. **(I)** Liver TC. **(J)** Liver TG. **(K)** Liver HDL. **(L)** Liver LDL. **(M)** Liver AKP. **(N)** Serum ALT. **(O)** Serum AST. **(P)** Serum TC. **(Q)** Serum TG. **(R)** Serum HDL. **(S)** Serum LDL. **(T)** Serum AKP. **(U)** Serum TBA. Data were expressed as mean ± SEM. **P*<0.05, ***P*<0.01, ****P*<0.001,*****P*<0.0001.

Figure 6. Ethanol-metabolizing lactobacilli isolated from alcohol-tolerant individuals reduce inflammation and restore ethanol-metabolizing enzyme function in alcoholic liver injury. (A) Liver TNF-α. **(B)** Liver IL-6. **(C)** Liver IL-1β. **(D)** Liver IL-10. **(E)** Serum TNF-α. **(F)** Serum IL-6. **(G)** Serum IL-1β. **(H)** Serum IL-10. **(I)** Liver ADH activity. **(J)** Liver ALDH activity. **(K)** Liver ADH protein level. **(L)** Liver ALDH protein level. **(M)** Serum ADH activity. **(N)** Serum ALDH activity. **(O)** Serum ADH protein level. **(P)** Serum ALDH protein level. Data were expressed as mean ± SEM. **P*<0.05, ***P*<0.01, ****P*<0.001,*****P*<0.0001.

Figure 7. NaB ameliorates alcohol-induced liver injury and metabolic dysregulation in mice. (A) Animals and experimental design (n=8 per group). (**B)** Body weight changes over time. **(C)** Food intake. **(D)** Blood glucose. **(E)** Liver weight. (**F)** Liver index (liver weight/body weight ratio). **(G)**Liver ALT:alanine aminotransferase. (**H)** Liver AST: aspartate aminotransferase. **(I)** Liver TC:total cholesterol. **(J)**Liver TG:triglyceride. **(K)** Liver HDL:High-Density Lipoprotein. **(L)** Liver LDL:Low-Density Lipoprotein. **(M)** Liver AKP:Alkaline Phosphatase. **(N)**Serum ALT. **(O)** Serum AST. **(P)** Serum TC. **(Q)** Serum TG. **(R)** Serum HDL. **(S)** Serum LDL. **(T)**Serum AKP. **(U)** Serum TBA: Total bile acids. Data were expressed as mean ± SEM. **P*<0.05, ***P*<0.01, ****P*<0.001,*****P*<0.0001.

Figure 8. NaB attenuates alcohol-induced hepatic injury, inflammation, and dysregulation of ethanol-metabolizing enzymes in mice. (A) Representative hematoxylin–eosin (H&E) staining of liver sections. **(B)** Liver tumor necrosis factor-α (TNF-α)**. (C)** Liver interleukin-6 (IL-6). **(D)** Liver interleukin-1β (IL-1β). **(E)** Liver interleukin-10 (IL-10). **(F)** Serum TNF-α. **(G)** Serum IL-6. **(H)** Serum IL-1β. **(I)** Serum IL-10. **(J)** Liver alcohol dehydrogenase (ADH) activity. **(K)** Liver aldehyde dehydrogenase (ALDH) activity. **(L)** Liver ADH protein level. **(M)** Liver ALDH protein leve. **(N)** Serum ADH activity. **(O)** Serum ALDH activity. **(P)** Serum ADH protein level. **(Q)** Serum ALDH protein level. Data were expressed as mean ± SEM. **P*<0.05, ***P*<0.01, ****P*<0.001,*****P*<0.0001.

Figure 9. NaB alleviates alcohol-induced intestinal barrier disruption and improves tight junction protein expression in mice. (A) Serum lipopolysaccharide (LPS) levels. **(B)** Representative hematoxylin–eosin (H&E) staining of colonic sections. **(C)** Immunofluorescence staining of tight junction proteins ZO-1 (green) and Occludin (red) in colonic tissues; nuclei stained with DAPI (blue); merged images shown in bottom row(n=3 per group). **(D)** Quantitative analysis of ZO-1 fluorescence intensity. **(E)** Quantitative analysis of Occludin fluorescence intensity. Data

were expressed as mean ± SEM. *P<0.05, **P<0.01, ***P<0.001,****P<0.0001.

Figure 10-1. NaB modulates gut microbiota composition and community structure in alcohol-fed mice. (A) Venn diagram of operational taxonomic units (OTUs) shared among groups. **(B)** Species accumulation curve presented as boxplots (n = 6 per group). **(C)** Rarefaction curves based on observed OTUs. **(D)** Species richness curves (observed OTUs) across groups. **(E)** Simpson index. **(F)** Shannon index. **(G)** Principal coordinate analysis (PCoA) plot based on Bray-Curtis distance. **(H)** Non-metric multidimensional scaling (NMDS) plot based on Bray-Curtis distance. **(I)** Relative abundance bar plot. **(J)** Hierarchical clustering heatmap and **(K)** chord diagram of gut microbial composition at the phylum level. **(L)** Relative abundance bar plot, **(M)** hierarchical clustering heatmap and **(N)** chord diagram of gut microbial composition at the genus level. **(O)** Differential abundance of gut microbial genera between CON and MOD groups, **(P)** between MOD and MOD+NaB groups, and **(Q)** between CON and CON+NaB groups. Data were expressed as mean ± SEM. *P<0.05, **P<0.01, ***P<0.001,****P<0.0001, n = 6 per group.

Figure 10-2. NaB reshapes gut microbial functional potential and enhances ethanol metabolism-associated pathways. (R) Linear discriminant analysis (LDA) effect size (LEfSe) results showing differentially abundant taxa. **(S)** Cladogram illustrating phylogenetic distribution of significantly discriminative microbial lineages identified by LEfSe. **(T-U)**Correlation networks of bacterial genera based on **(T)** Spearman's rank correlation and **(U)** Pearson's correlation ($|r| > 0.6$, $P < 0.05$). **(V-W)** Relative abundance of key microbial enzyme functions related to alcohol metabolism based on KEGG EC numbers: **(V)** EC 1.1.1.1 (alcohol dehydrogenase) and **(W)** EC 1.2.1.3 (aldehyde dehydrogenase). **(X)** Predicted KEGG pathway profiles using PICRUSt2 (level 2). **(Y)** Top 35 KEGG Level 3 pathways ranked by overall mean relative abundance. Data were expressed as mean ± SEM. *P<0.05, **P<0.01, ***P<0.001,****P<0.0001, n = 6 per group.

Figure 11. Spearman correlation analysis reveals associations between gut microbial genera and host inflammatory, and liver function parameters in alcohol-fed mice. (A) Correlation heatmap between bacterial genera and key physiological and biochemical indicators of ALD. **(B)** Correlation heatmap between bacterial genera and inflammatory cytokines and alcohol metabolism enzymes. **(C)** Correlation heatmap among host clinical parameters. Data are presented as Spearman's correlation coefficients (r), with color intensity representing the strength and direction of correlation (red: positive; blue: negative). *P<0.05, **P<0.01, ***P<0.001, ****P<0.0001, n = 6-8 per group.

Figure 12. The hepatoprotective effects of NaB are dependent on gut microbiota integrity in alcohol-fed mice. (A) Experimental design and animal groups (n = 8 per group). **(B)** Body weight changes over time. **(C)** Food intake. **(D)** Blood glucose. **(E)** Liver weight. **(F)** Liver index. **(G)** Liver ALT. **(H)** Liver AST. **(I)** Liver TC. **(J)** Liver TG. **(K)** Liver HDL. **(L)** Liver LDL. **(M)** Liver AKP. **(N)** Serum ALT. **(O)** Serum AST. **(P)** Serum TC. **(Q)** Serum TG. **(R)** Serum HDL. **(S)** Serum LDL. **(T)** Serum AKP**(U)** Serum TBA. Data were expressed as mean ± SEM. *P<0.05, **P<0.01,

P<0.001,*P<0.0001.

Figure 13. NaB attenuates alcohol-induced hepatic injury, inflammation, and dysregulation of ethanol-metabolizing enzymes in mice, with effects dependent on gut microbiota integrity. **(A)** H&E staining of liver sections. **(B)** Liver TNF-α. **(C)** Liver IL-6. **(D)** Liver IL-1β. **(E)** Liver IL-10. **(F)** Serum TNF-α. **(G)** Serum IL-6. **(H)** Serum IL-1β **(I)** Serum IL-10. **(J)** Liver ADH activity. **(K)** Liver ALDH activity. **(L)** Liver ADH protein level. **(M)** Liver ALDH protein level. **(N)** Serum ADH activity. **(O)** Serum ALDH activity. **(P)** Serum ADH protein level. **(Q)** Serum ALDH protein level. Data were expressed as mean ± SEM. *P<0.05, **P<0.01, ***P<0.001, ****P<0.0001.

Figure 14. NaB improves intestinal barrier integrity and tight junction protein expression in alcohol-fed mice, with effects dependent on gut microbiota integrity. **(A)** H&E staining of colonic sections. **(B)** Immunofluorescence staining of tight junction proteins ZO-1 (green) and Occludin (red) in colonic tissues; nuclei stained with DAPI (blue); merged images shown in bottom row (n = 3 per group). **(C)** Quantitative analysis of ZO-1 fluorescence intensity. **(D)** Quantitative analysis of Occludin fluorescence intensity. Data were expressed as mean ± SEM. *P<0.05, **P<0.01, ***P<0.001,****P<0.0001.

Figure 15. NaB synergizes with ethanol-metabolizing lactobacilli to ameliorate alcoholic liver disease. **(A)** Experimental design and animal groups (n = 8 per group). **(B)** Body weight changes over time. **(C)** Food intake. **(D)** Blood glucose. **(E)** Liver weight. **(F)** Liver index. **(G)** Liver ALT. **(H)** Liver AST. **(I)** Liver TC. **(J)** Liver TG. **(K)** Liver HDL. **(L)** Liver LDL. **(M)** Liver AKP. **(N)** Serum ALT. **(O)** Serum AST. **(P)** Serum TC. **(Q)** Serum TG. **(R)** Serum HDL. **(S)** Serum LDL. **(T)** Serum AKP. **(U)** Serum TBA. Data were expressed as mean ± SEM. *P<0.05, **P<0.01, ***P<0.001,****P<0.0001.

Figure 16. NaB synergizes with ethanol-metabolizing lactobacilli to ameliorate hepatic inflammation and enhance ethanol metabolism in alcoholic liver disease. **(A)** Liver TNF-α. **(B)** Liver IL-6. **(C)** Liver IL-1β. **(D)** Liver IL-10. **(E)** Serum TNF-α. **(F)** Serum IL-6. **(G)** Serum IL-1β. **(H)** Serum IL-10. **(I)** Liver ADH activity. **(J)** Liver ALDH activity. **(K)** Liver ADH protein level. **(L)** Liver ALDH protein level. **(M)** Serum ADH activity. **(N)** Serum ALDH activity. **(O)** Serum ADH protein level. **(P)** Serum ALDH protein level. Data were expressed as mean ± SEM. *P<0.05, **P<0.01, ***P<0.001,****P<0.0001.

Figure 17. NaB and ethanol-metabolizing lactobacilli ameliorate alcohol-induced histopathological damage in liver and colon. **(A)** H&E staining of liver sections. **(B)** H&E staining of colonic sections.

Figure 18. NaB synergizes with ethanol-metabolizing lactobacilli to restore intestinal tight junction proteins in alcoholic liver disease. **(A)** Immunofluorescence staining of ZO-1 (green) and Occludin (red) in colonic tissues; nuclei stained with DAPI (blue). Merged images shown in bottom

row. **(B)** Quantification analysis of ZO-1 fluorescence intensity. **(C)** Quantification analysis of Occludin fluorescence intensity.

Figure 19. Schematic representation of the experimental workflow and proposed mechanism by which sodium butyrate and ethanol-metabolizing lactobacilli protect against alcoholic liver disease via gut-liver axis modulation.

S 1. Taxonomic identification results of 91 purified bacterial isolates using mass pectrometry. Following two rounds of ethanol tolerance screening, we employed matrix-assisted laser desorption/ionization time-of-flight mass spectrometry (MALDI-TOF MS) to tentatively identify 91 ethanol-tolerant candidate isolates. Analysis revealed that the vast majority of these isolates belonged to the genus *Lactobacillus*.

S 2. Time-course analysis of ethanol degradation rate over 48 hours for 91 purified bacterial isolates. Based on the 48-hour ethanol degradation efficiency assay, we observed that all 71 isolates exhibited slow ethanol metabolism, with degradation rates remaining below 10% at the 48-hour time point.

S 3. Additional data supporting gastrointestinal stress tolerance screening. (A) Bile salt tolerance assay under 3% and 5% bile salt concentrations at four time points (2, 4, 6, and 8 h). **(B)** Acid tolerance assay under pH 2.0 and pH 3.0 conditions at three time points (2, 4, and 6 h).

S 4. Genomic and functional annotation of other candidate strains. (A) Circular genome maps of other candidate strains, with ethanol-metabolizing genes highlighted. **(B)** Top 30 predicted KEGG pathways. **(C)** Heatmap of CAZy classes. **(D)** Bar plot of CAZy classes. **(E)** Heatmap of all CAZy families.

S 5 Gram staining of other candidate strains. Following Gram staining, the candidate strains predominantly exhibited a violet coloration and a rod or short-rod morphology, consistent with their classification as Gram-positive bacteria. However, occasional heterogeneity or faint pink discoloration was observed in a subset of isolates, including M8, M1C, and MF.

S 6 Growth curves of other candidate isolates under ethanol-free and ethanol-stressed (15%) conditions, with or without NaB supplementation. In the absence of ethanol, NaB exerted a modest proliferative effect on strains MB, MD, ME, MF, M1C, M8, M15, T11, and T21. Upon exposure to a 15% (v/v) ethanol challenge, growth inhibition was observed across all strains; notably, NaB treatment failed to elicit a significant recovery in the growth of the aforementioned isolates.

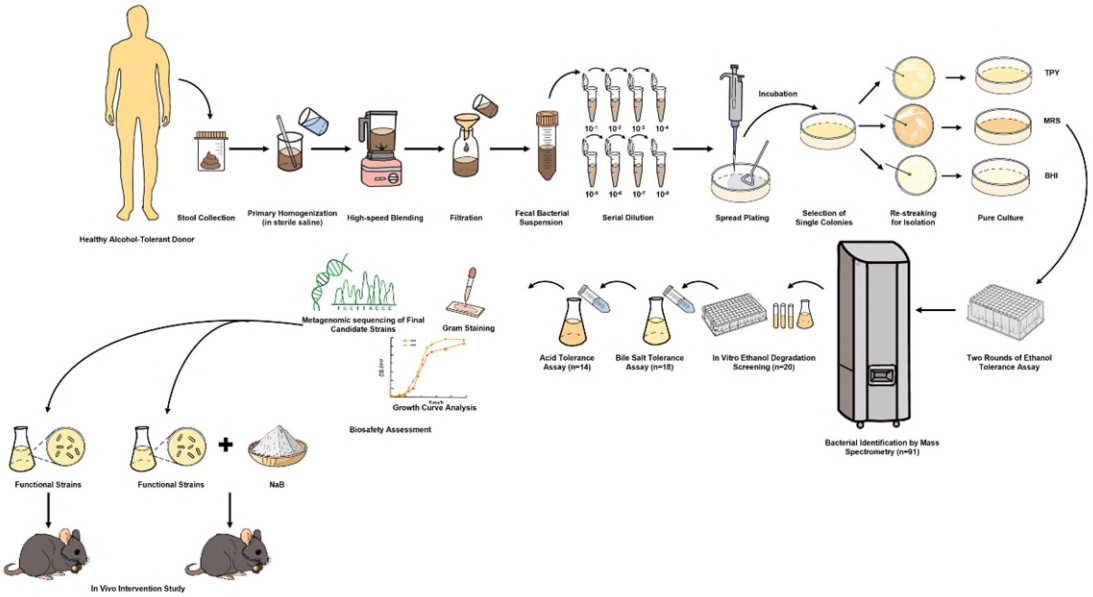


Figure 1. Isolation and functional characterization of ethanol-metabolizing gut bacteria from alcohol-tolerant individuals.

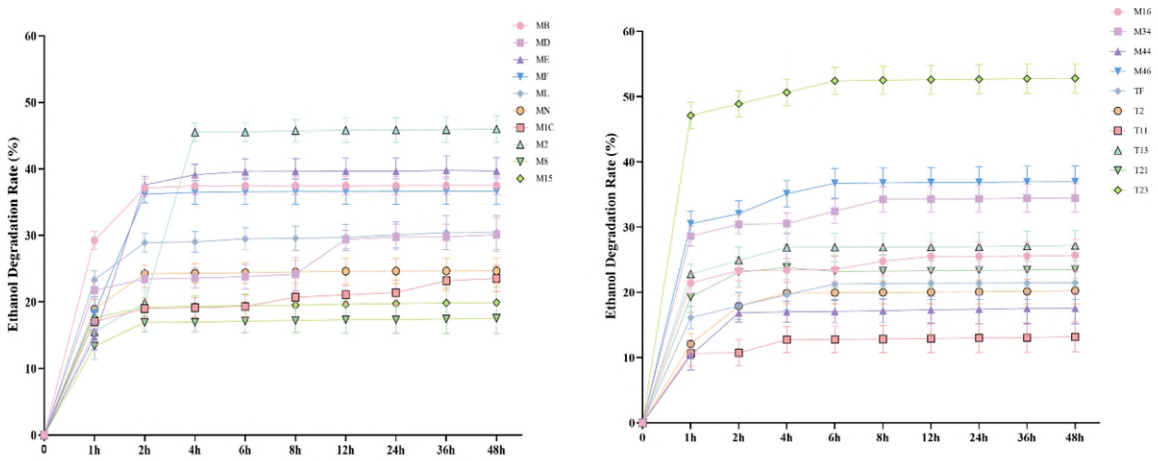


Figure 2. Time-course analysis of ethanol degradation rate over 48 hours for 91 purified bacterial isolates.

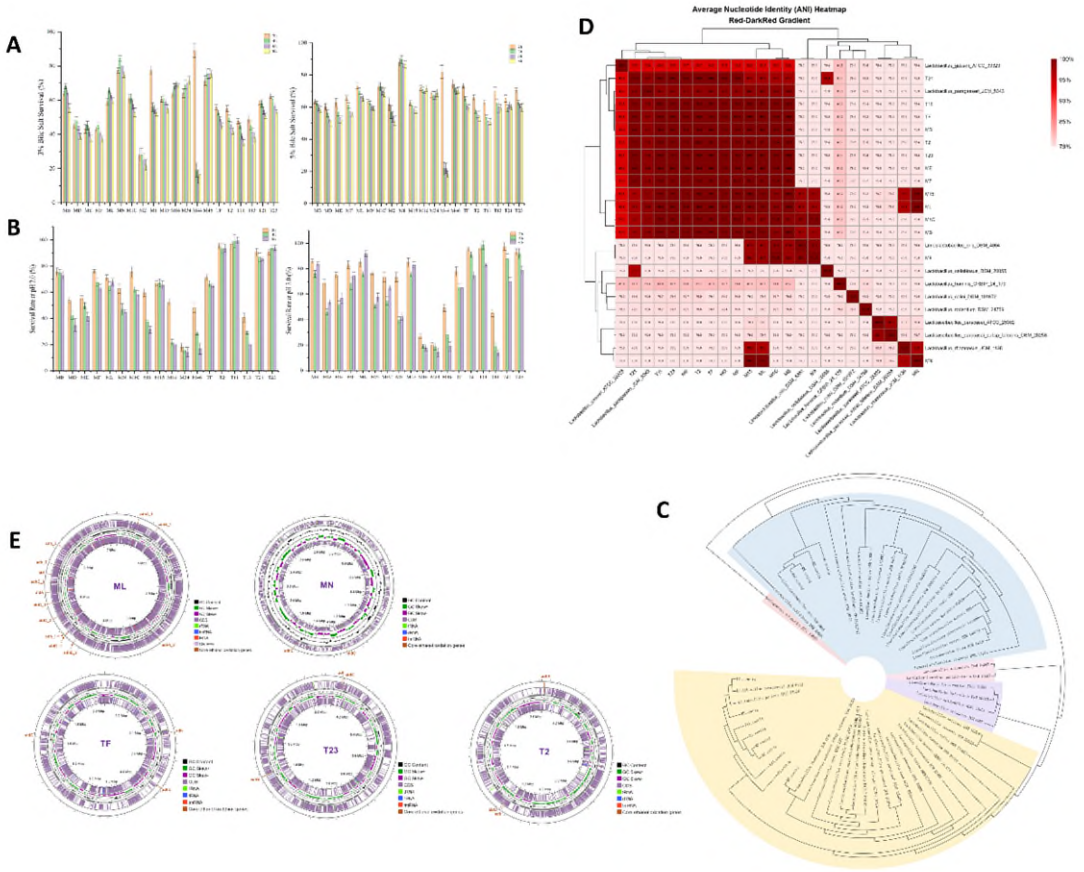


Figure 3-1. Taxonomic identification, and genomic characterization of ethanol-metabolizing bacterial strains from healthy alcohol-tolerant individuals.

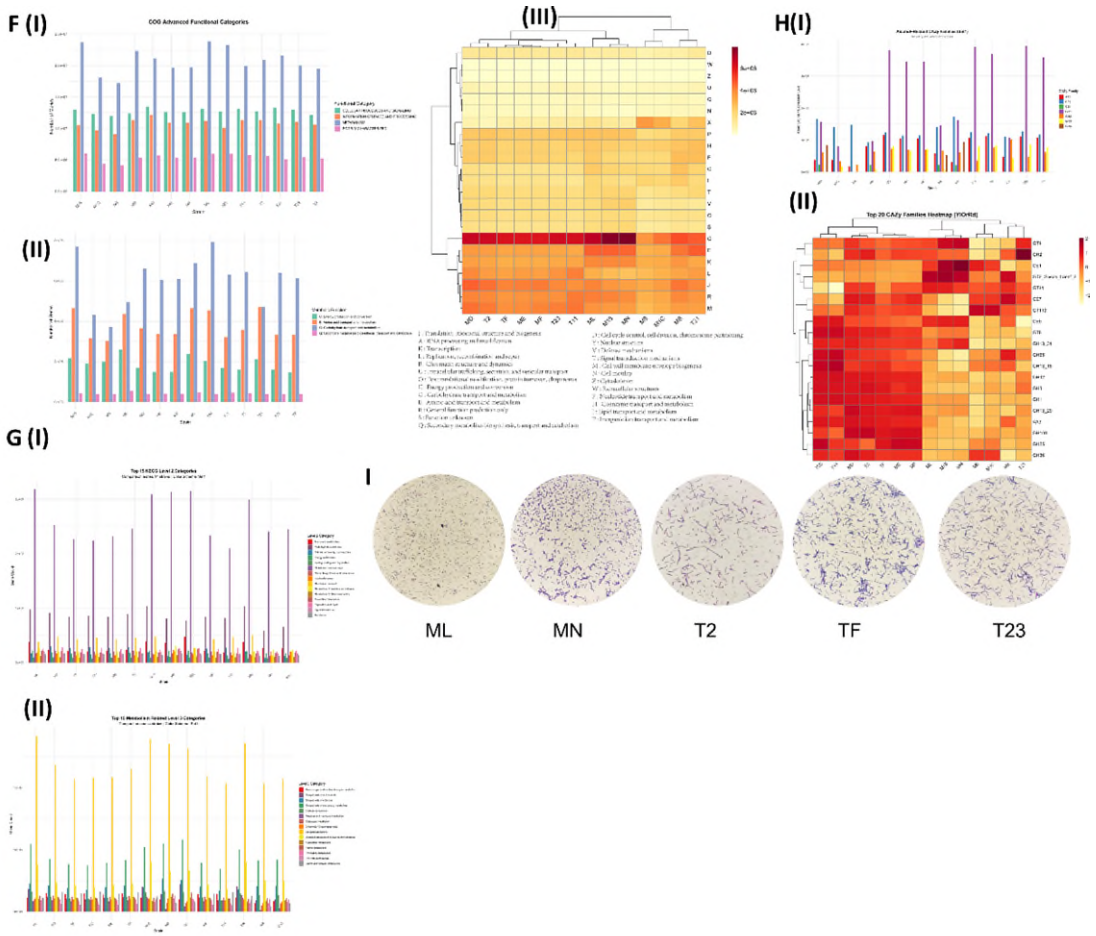


Figure 3-2. In vitro functional annotation of candidate strains.

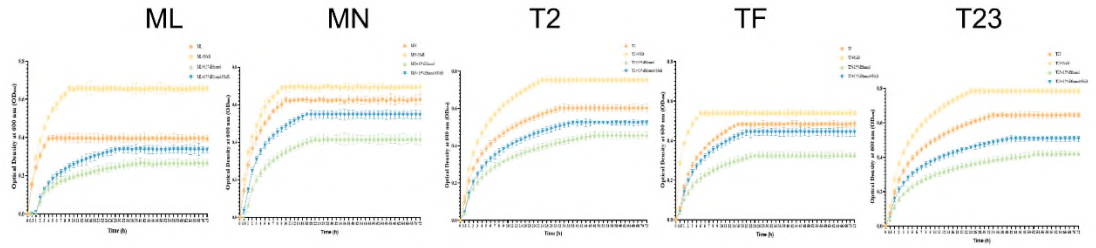


Figure 4. Growth kinetics under ethanol-free or 15% ethanol conditions with or without NaB.

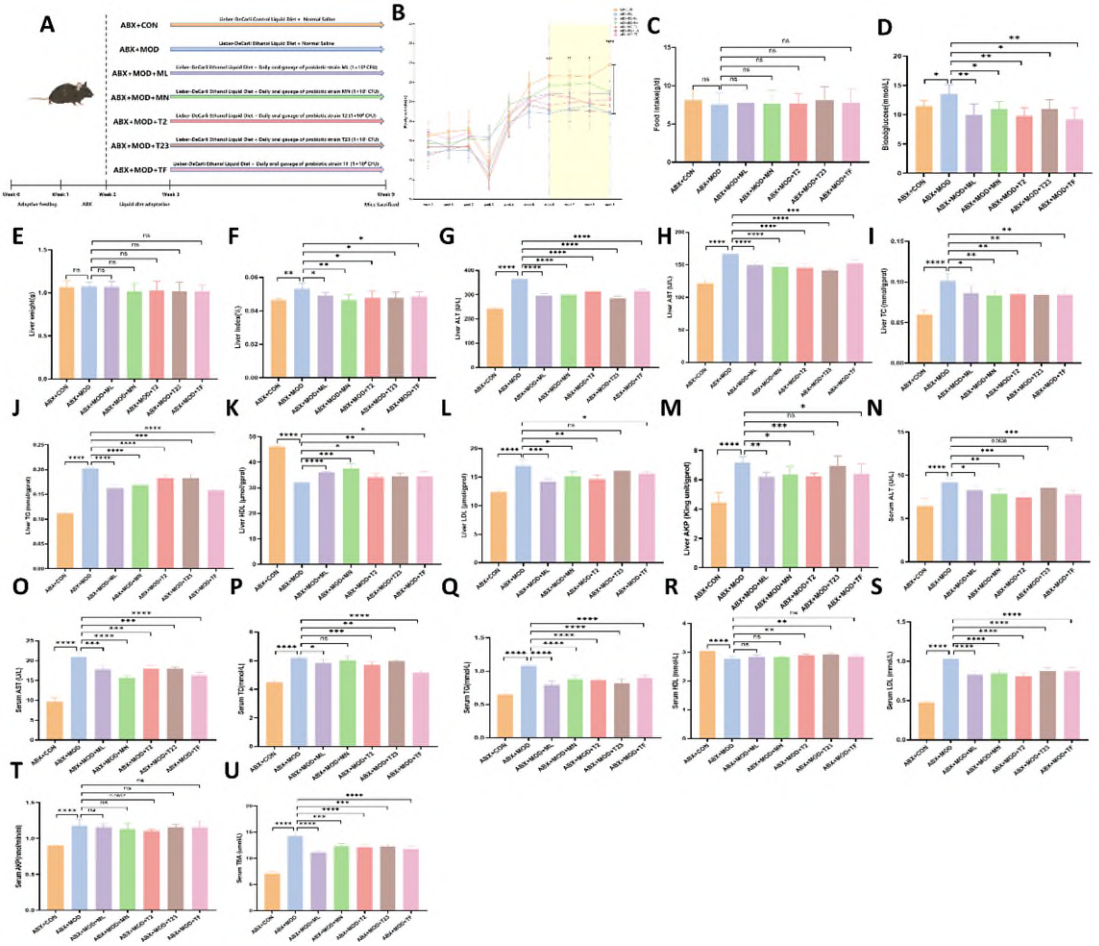


Figure 5. Ethanol-metabolizing lactobacilli isolated from alcohol-tolerant individuals protect against alcoholic liver injury in microbiota-depleted mice.

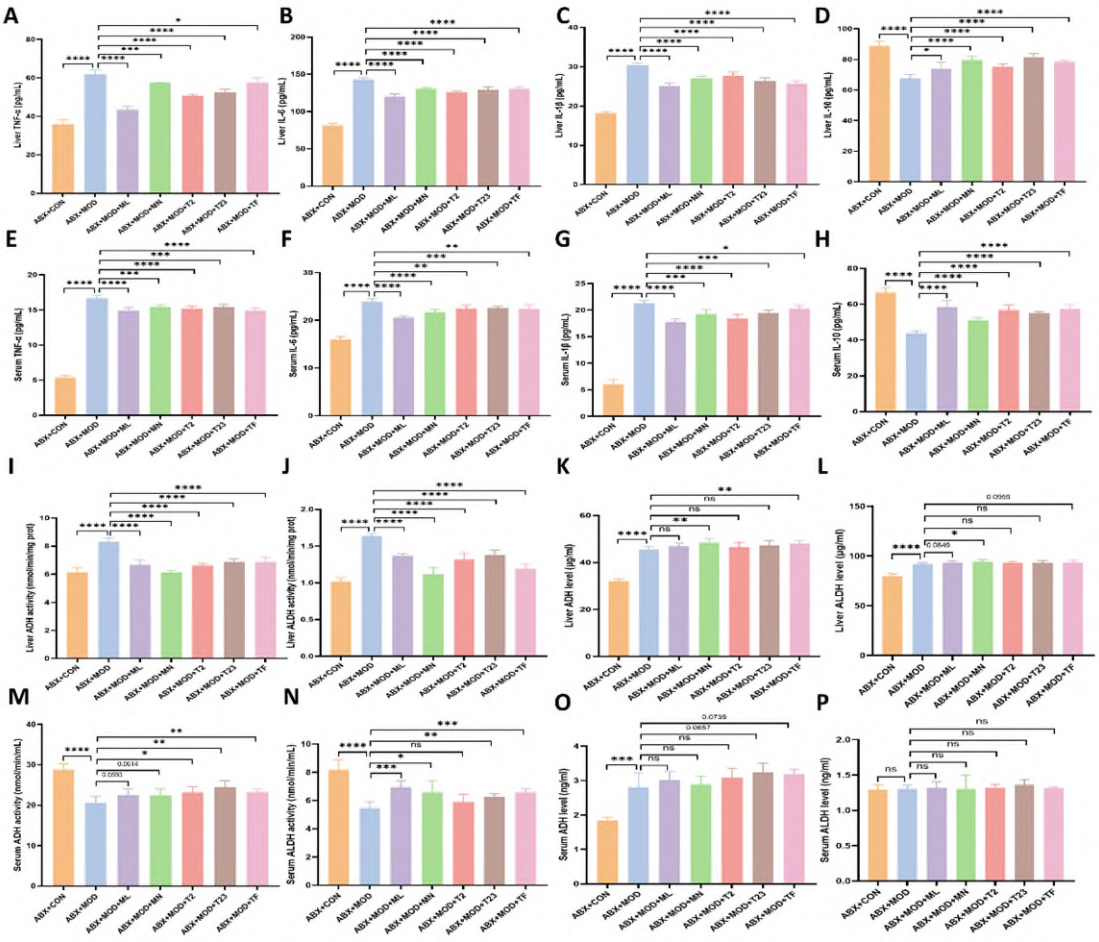


Figure 6. Ethanol-metabolizing lactobacilli isolated from alcohol-tolerant individuals reduce inflammation and restore ethanol-metabolizing enzyme function in alcoholic liver injury.

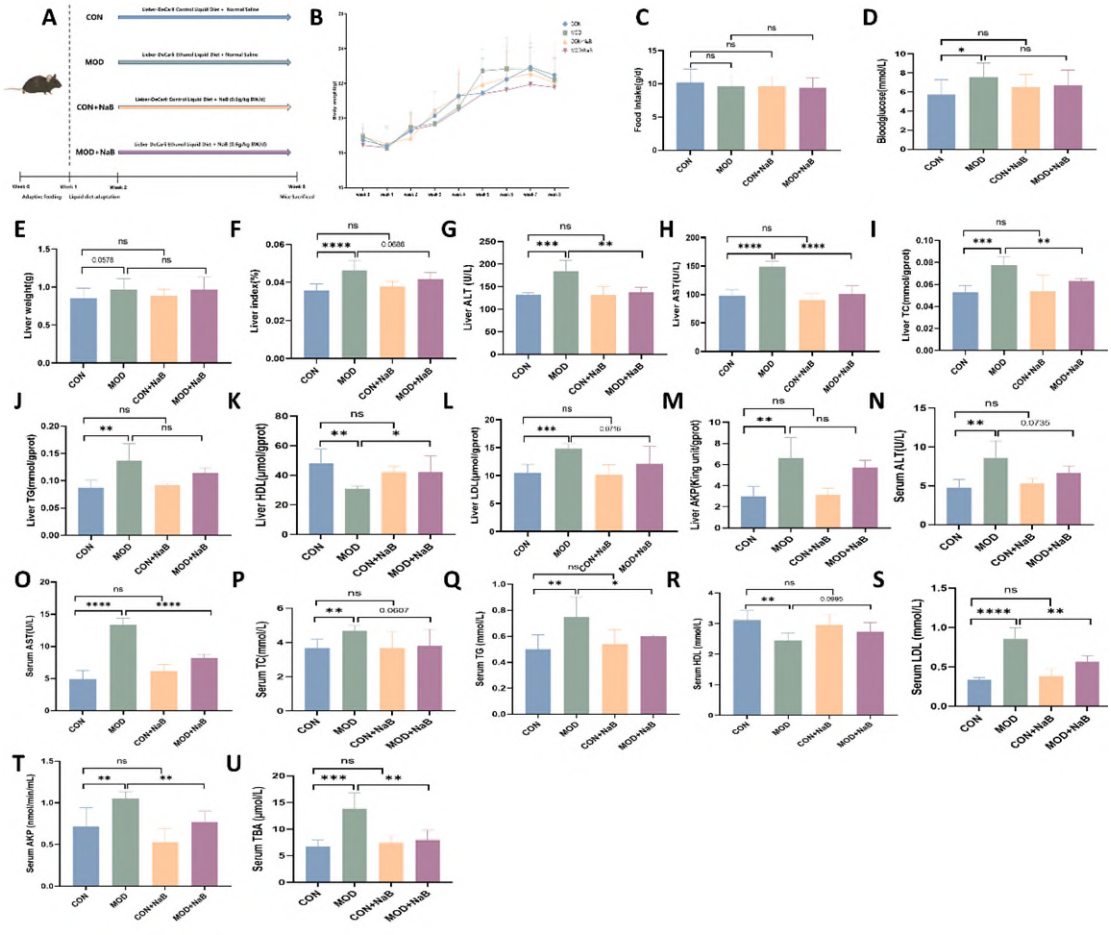


Figure 7. NaB ameliorates alcohol-induced liver injury and metabolic dysregulation in mice.

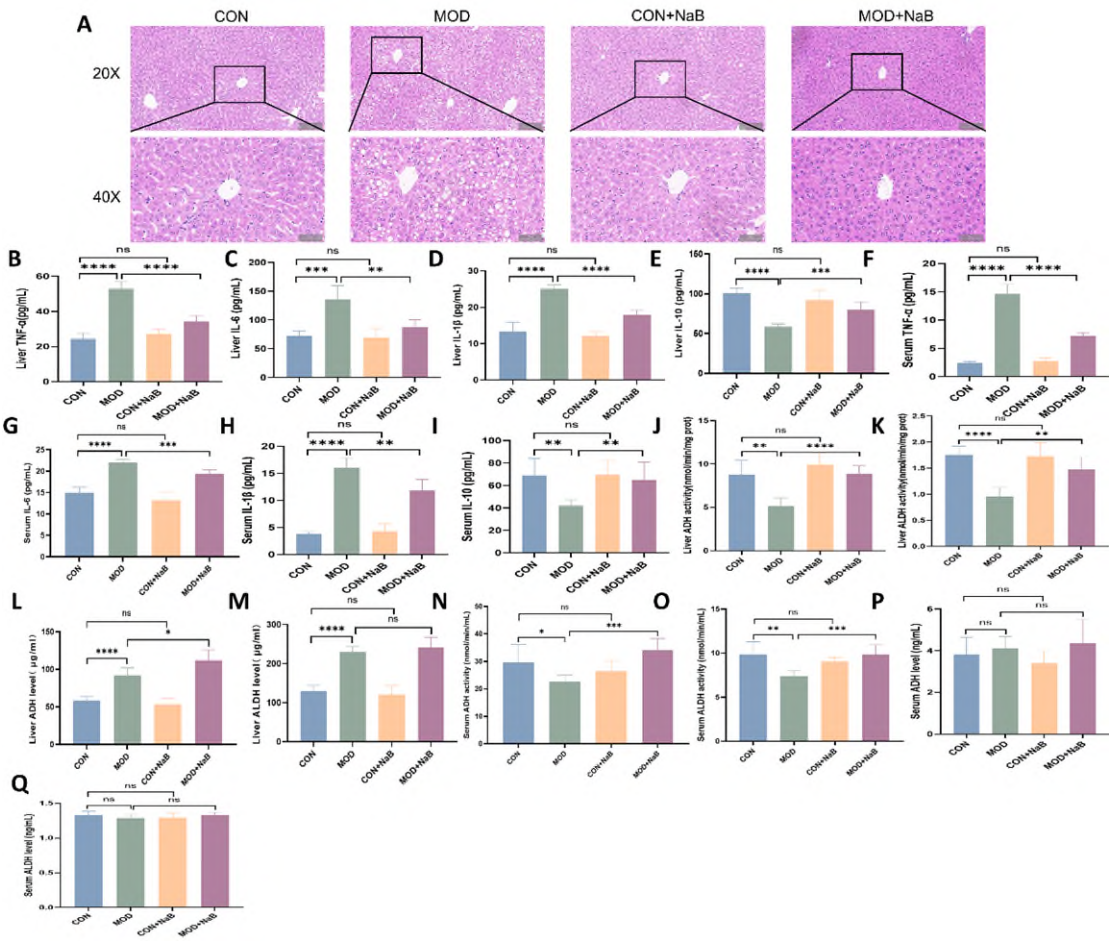


Figure 8. NaB attenuates alcohol-induced hepatic injury, inflammation, and dysregulation of ethanol-metabolizing enzymes in mice.

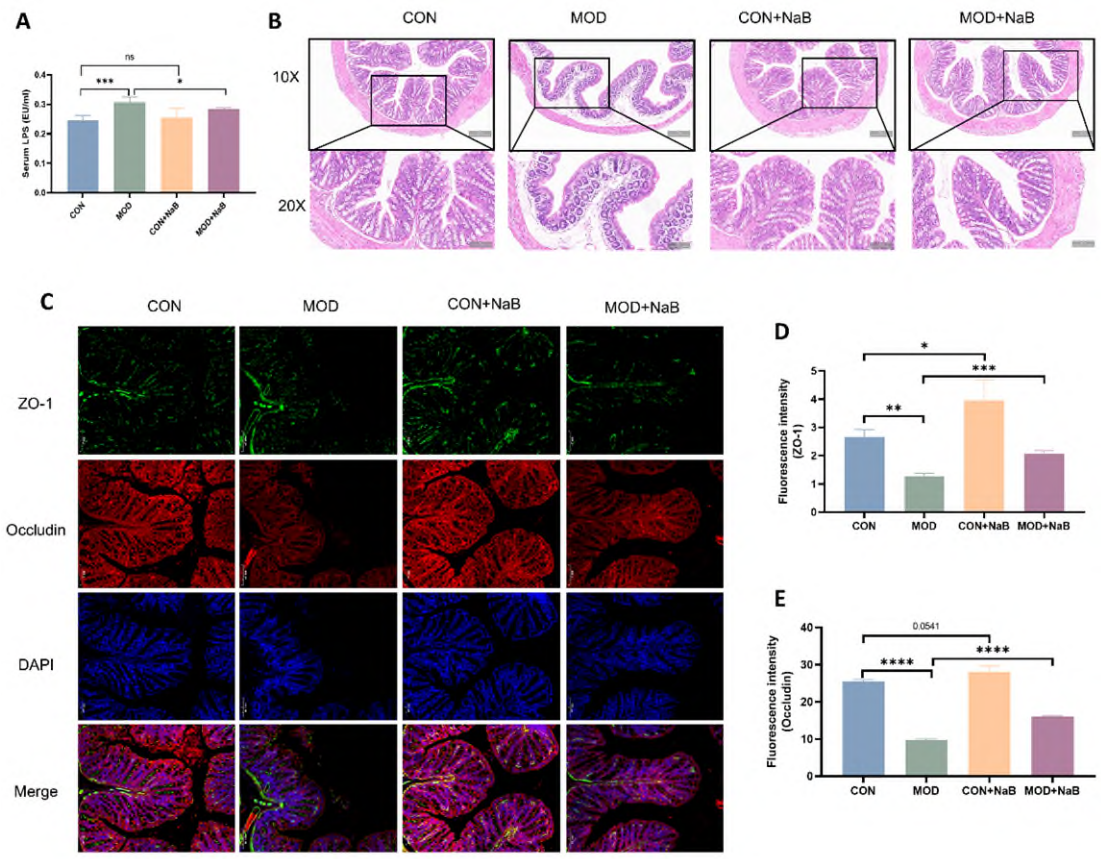


Figure 9. NaB alleviates alcohol-induced intestinal barrier disruption and improves tight junction protein expression in mice.

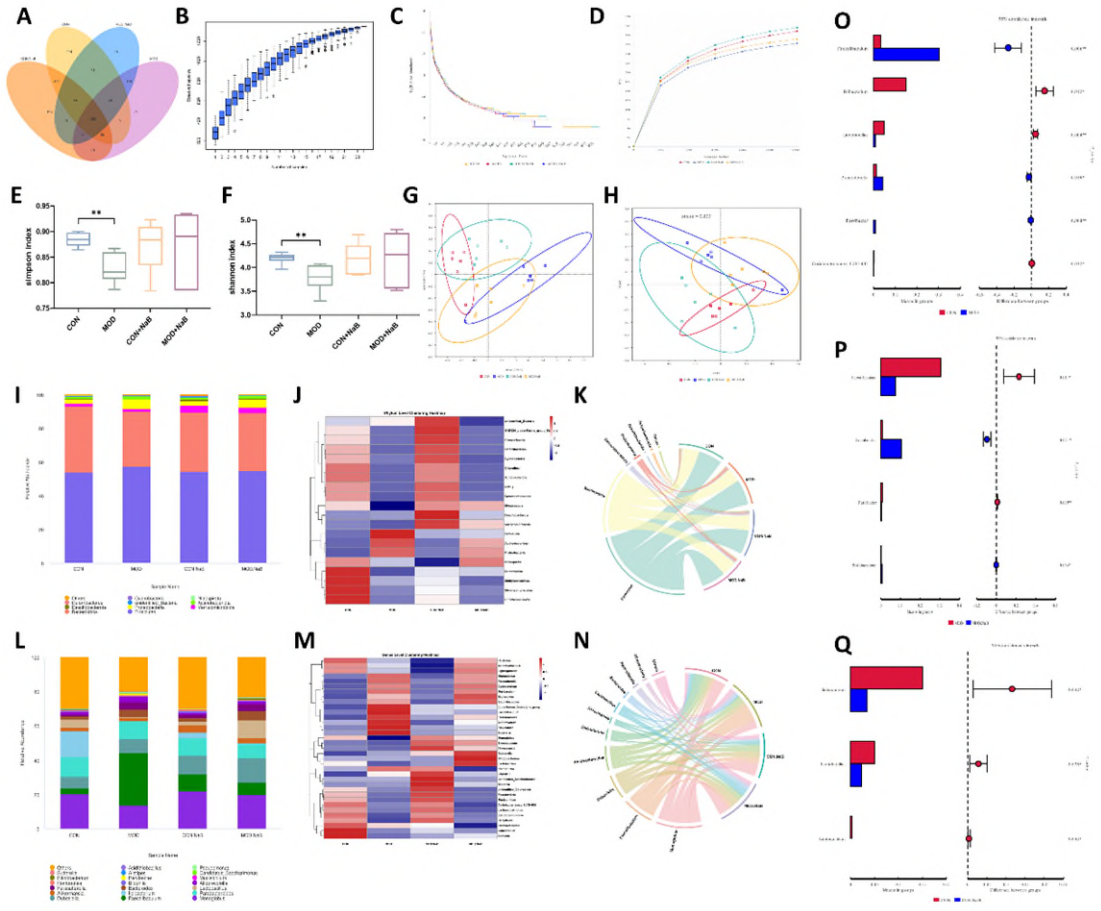


Figure 10-1. NaB modulates gut microbiota composition and community structure in alcohol-fed mice.

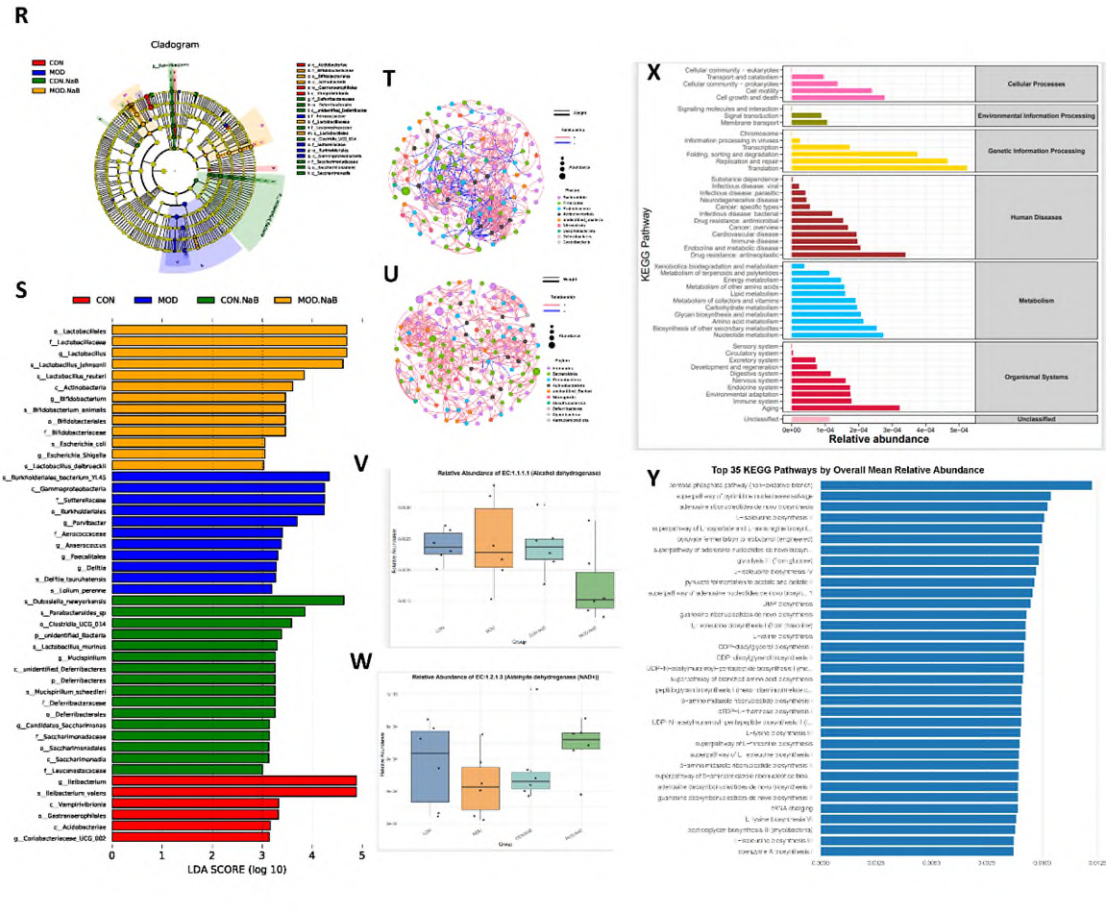


Figure 10-2. NaB reshapes gut microbial functional potential and enhances ethanol etabolism-associated pathways.

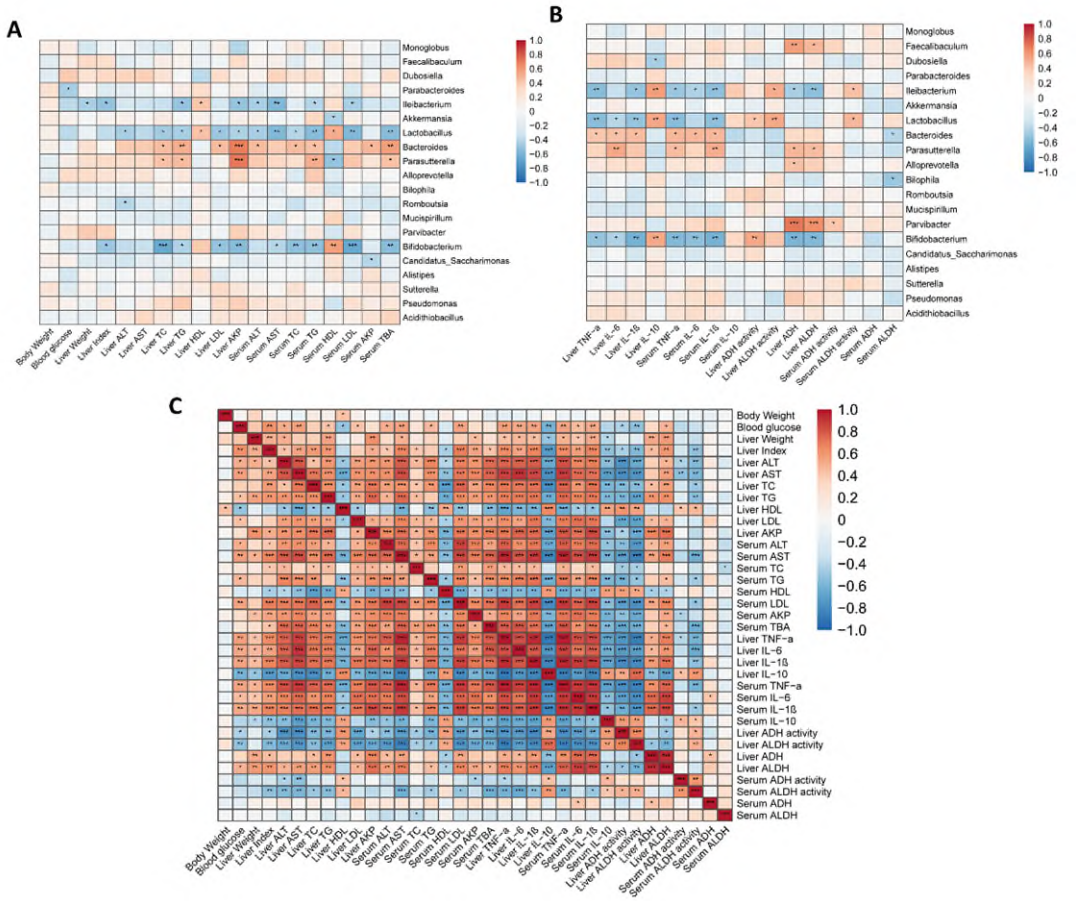


Figure 11. Spearman correlation analysis reveals associations between gut microbial genera and host inflammatory, and liver function parameters in alcohol-fed mice.

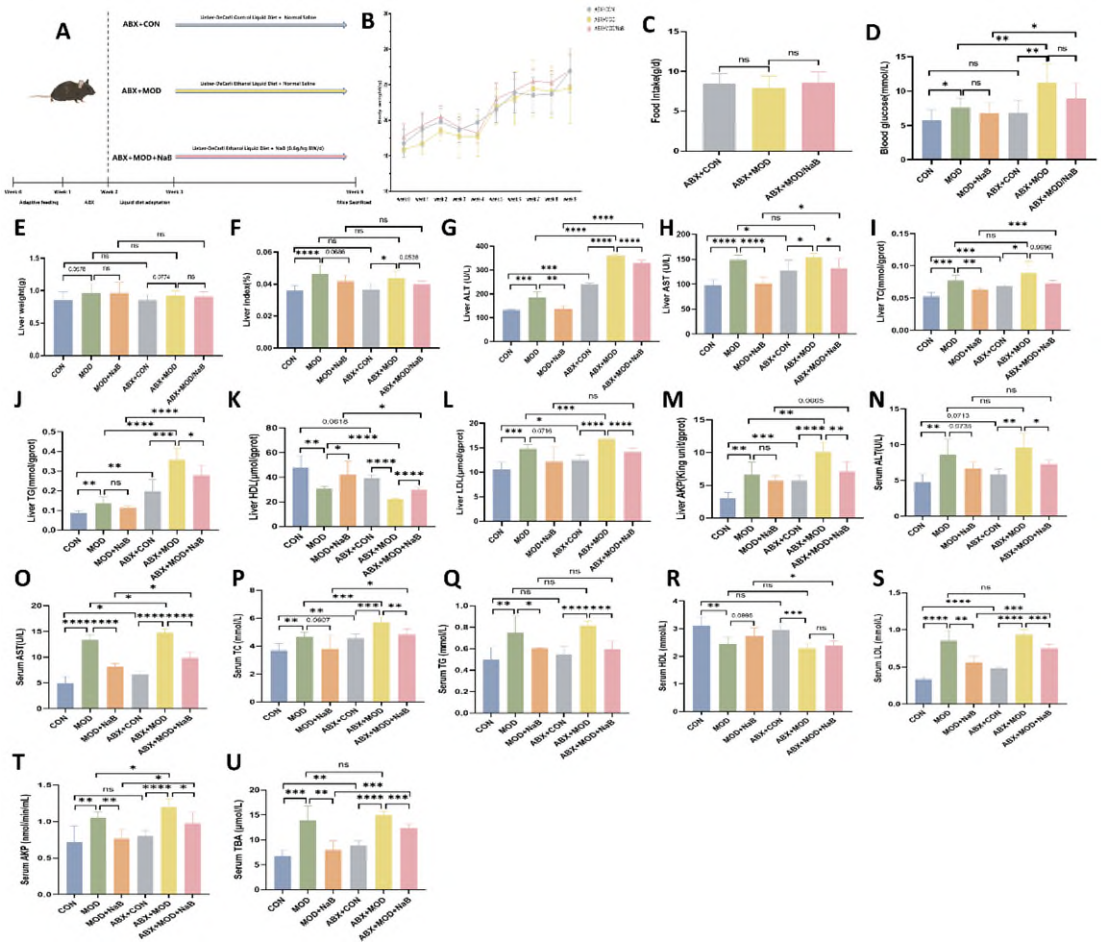


Figure 12. The hepatoprotective effects of NaB are dependent on gut microbiota integrity in alcohol-fed mice.

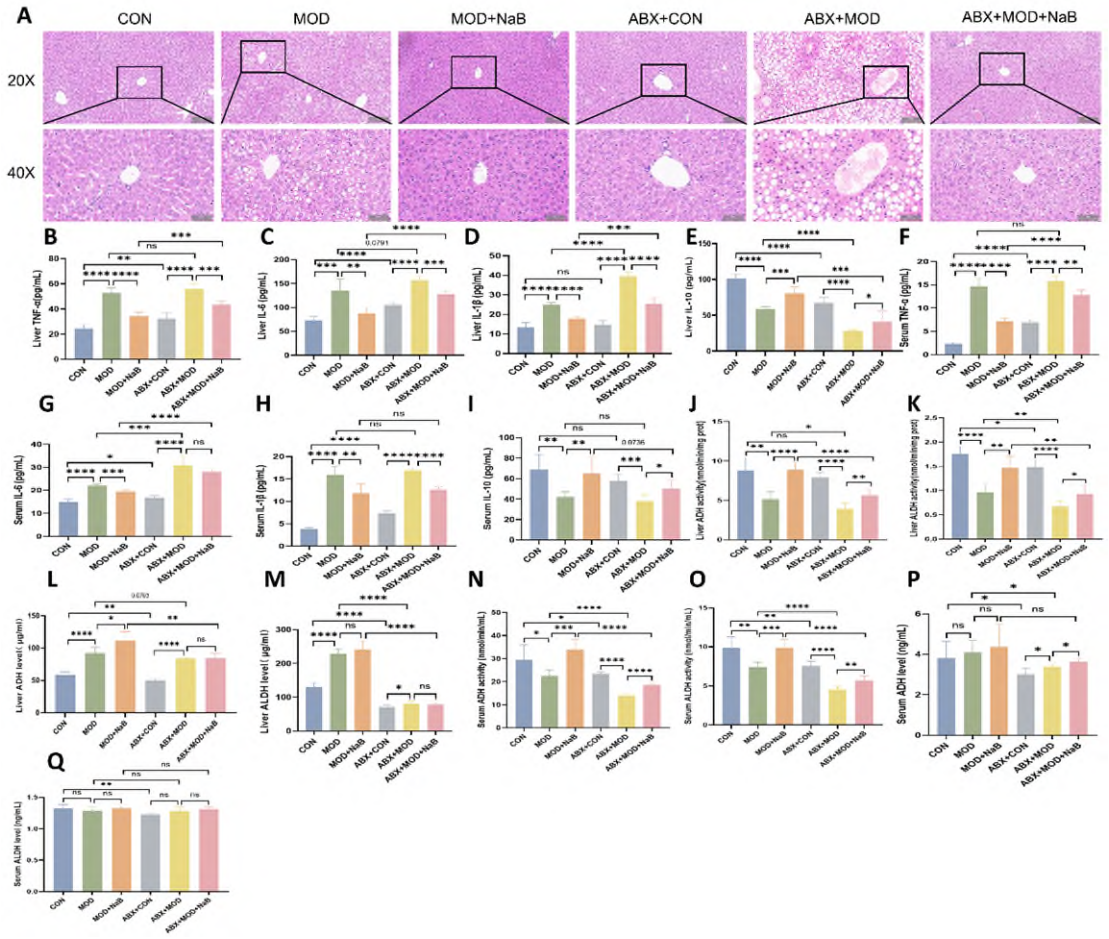


Figure 13. NaB attenuates alcohol-induced hepatic injury, inflammation, and dysregulation of ethanol-metabolizing enzymes in mice, with effects dependent on gut microbiota integrity.

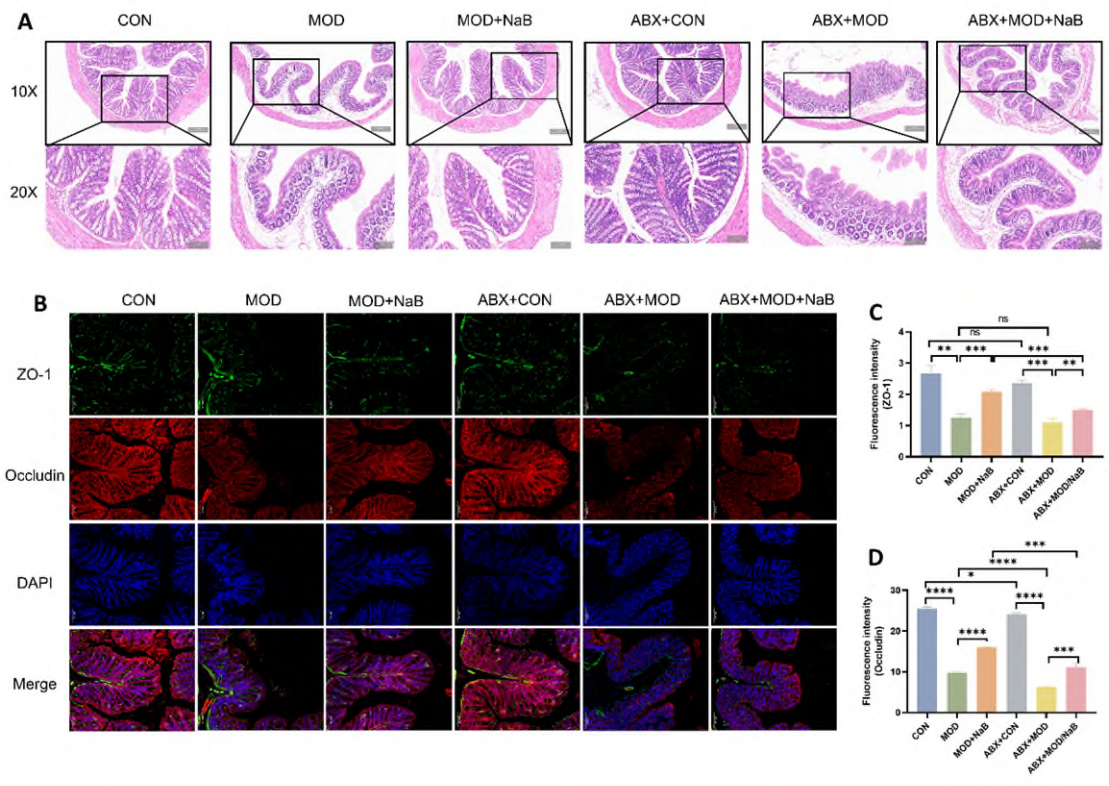


Figure 14. NaB improves intestinal barrier integrity and tight junction protein expression in alcohol-fed mice, with effects dependent on gut microbiota integrity.

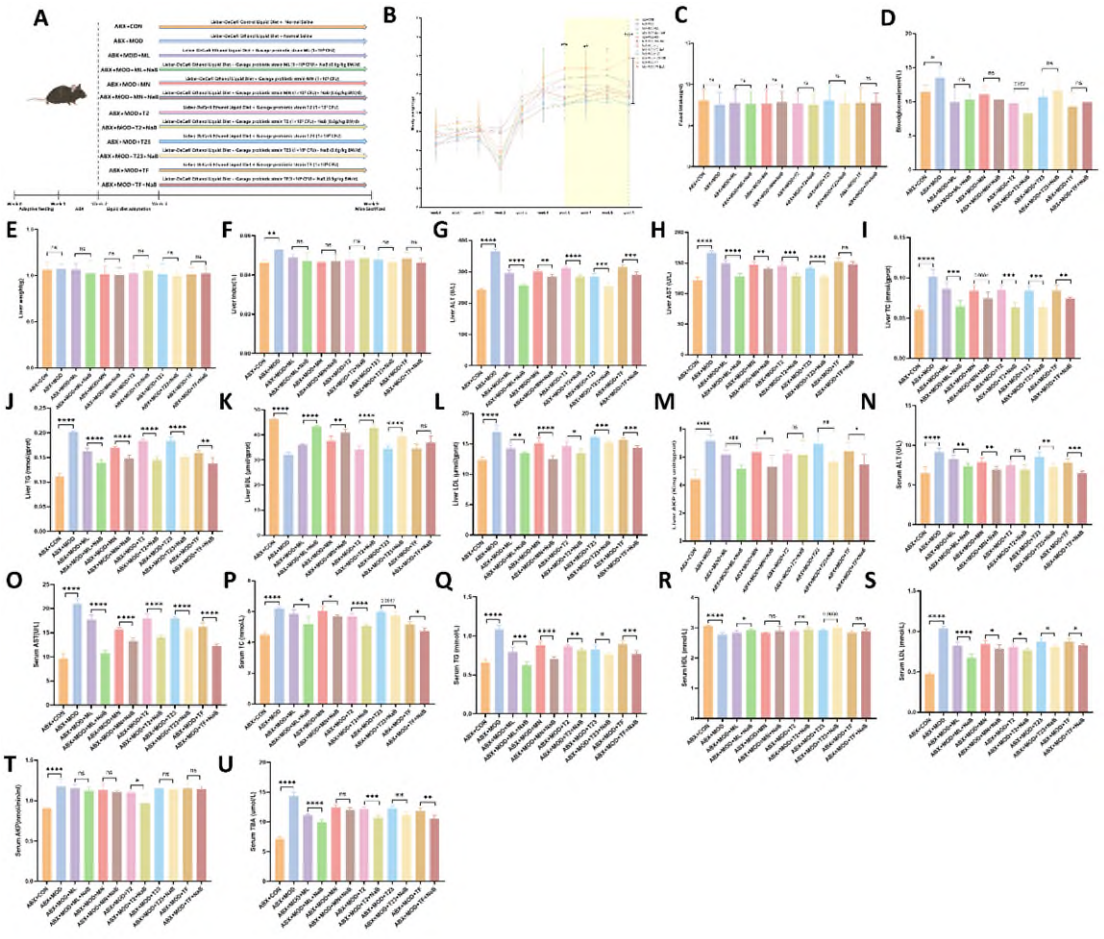


Figure 15. NaB synergizes with ethanol-metabolizing lactobacilli to ameliorate alcoholic liver disease.

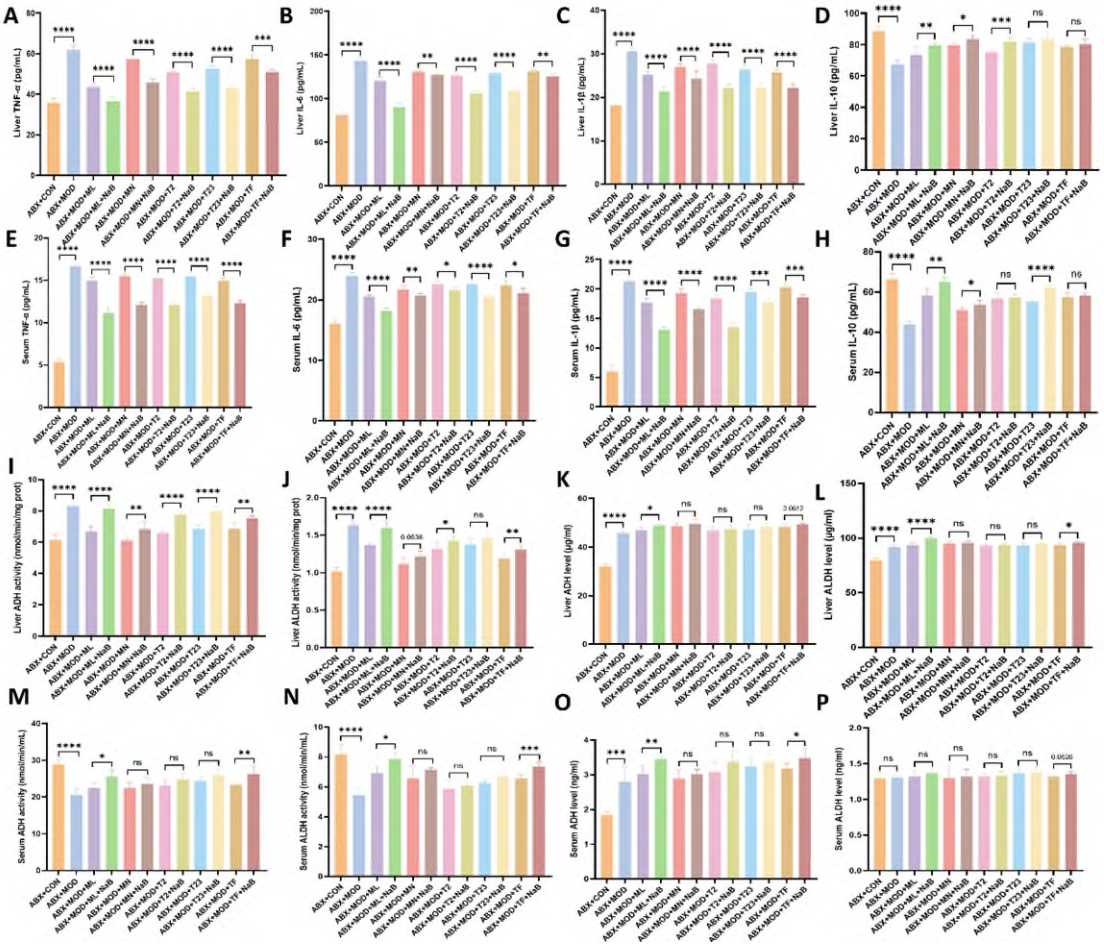


Figure 16. NaB synergizes with ethanol-metabolizing lactobacilli to ameliorate hepatic inflammation and enhance ethanol metabolism in alcoholic liver disease.

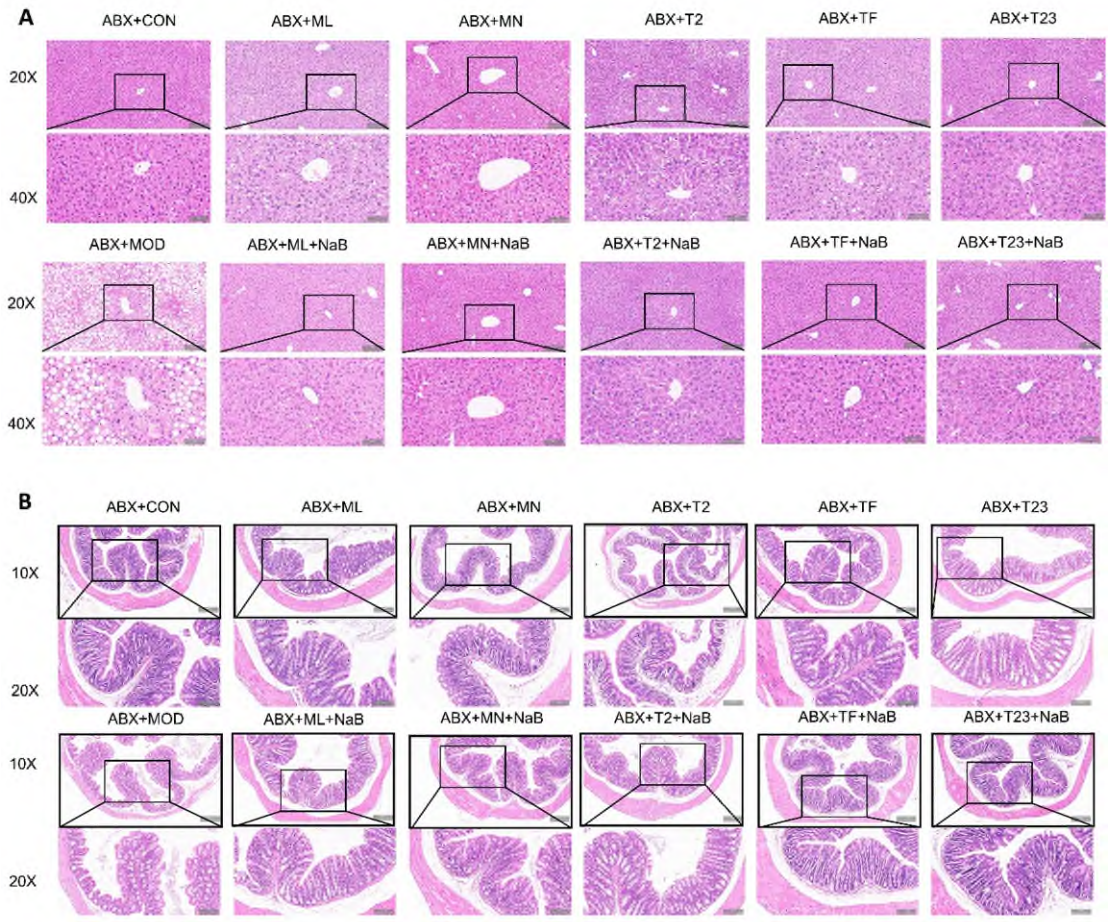


Figure 17. NaB and ethanol-metabolizing lactobacilli ameliorate alcohol-induced histopathological damage in liver and colon.

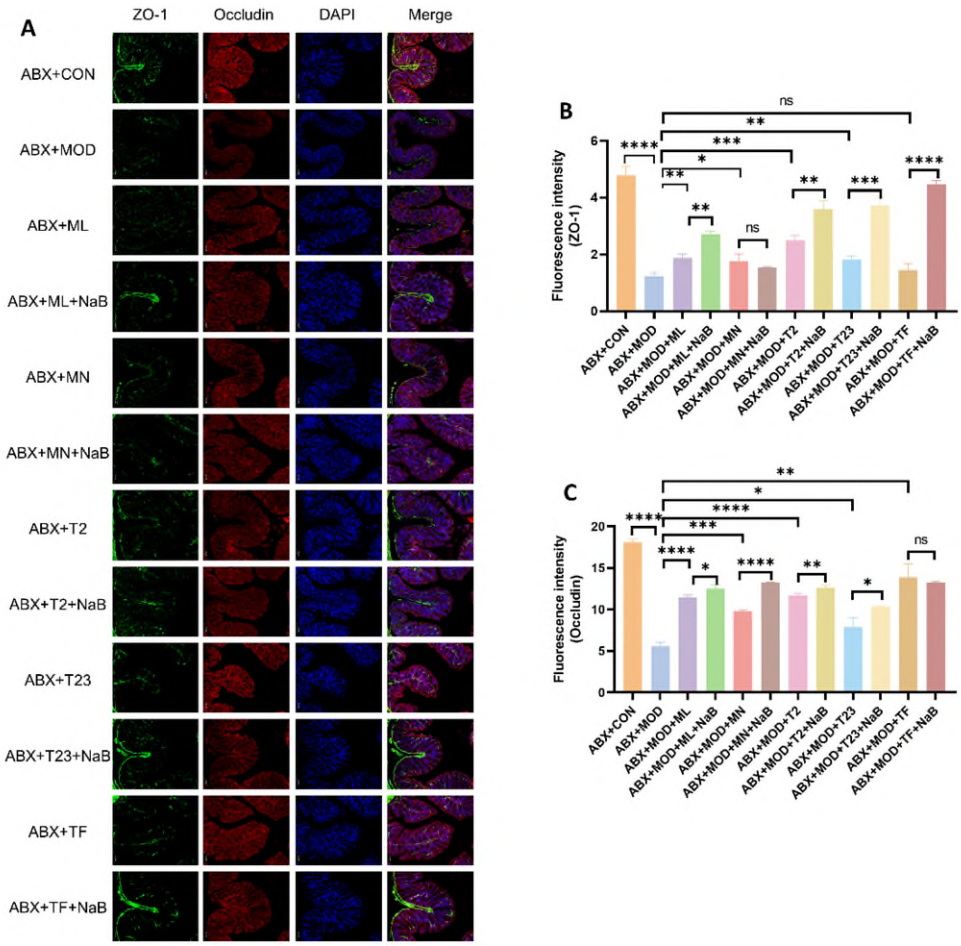


Figure 18. NaB synergizes with ethanol-metabolizing lactobacilli to restore intestinal tight junction proteins in alcoholic liver disease.

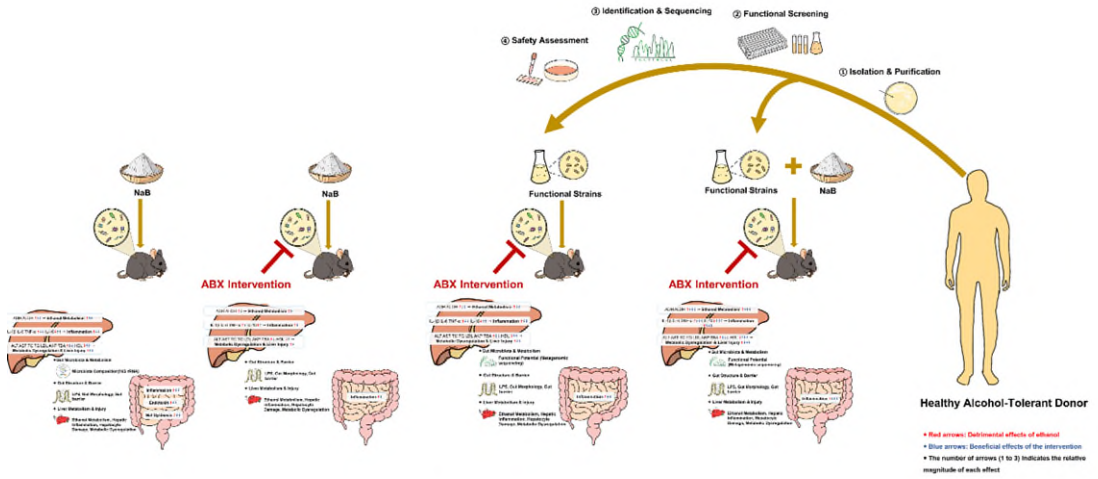


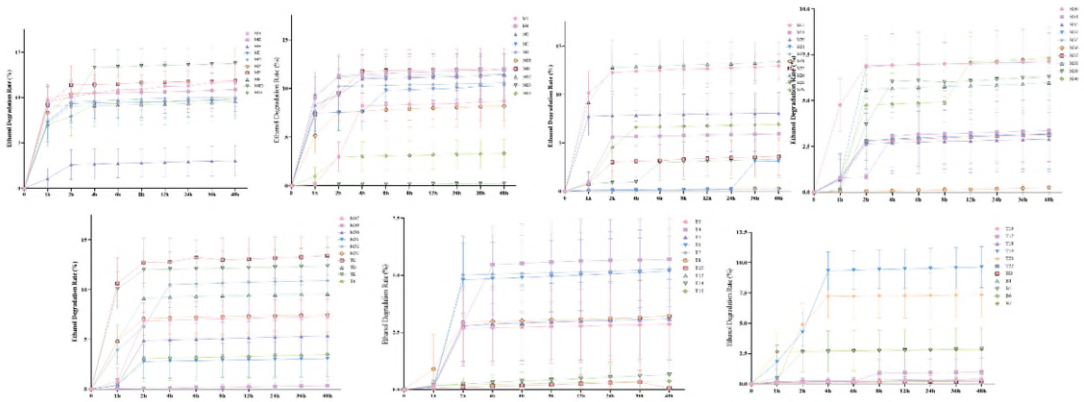
Figure 19. Schematic representation of the experimental workflow and proposed mechanism by which sodium butyrate and ethanol-metabolizing lactobacilli protect against alcoholic liver disease via gut-liver axis modulation.

number	Study identifier	Identification results	number of positive results	Identification results	number of positive results	number	Study identifier	Identification results	number of positive results	Identification results	number of positive results
1	MA	*Lactobacillus casei/paracasei/rhamnosus*	3	*Lactobacillus acidophilus/gasseri*	3	16	M1E	*Lactobacillus acidophilus/gasseri*	4		
2	MB	*Lactobacillus acidophilus/gasseri*	3			17	M1	*Lactobacillus acidophilus/gasseri*	3		
3	MD	*Lactobacillus acidophilus/gasseri*	4			18	M2	*Lactobacillus acidophilus/gasseri*	4		
4	ME	*Lactobacillus acidophilus/gasseri*	4			19	M4	*Lactobacillus acidophilus/gasseri*	4		
5	MF	*Lactobacillus acidophilus/gasseri*	4			20	M6	*Lactobacillus acidophilus/gasseri*	2		
6	MG	*Lactobacillus acidophilus/gasseri*	2			21	M7	*Lactobacillus acidophilus/gasseri*	4		
7	MH	*Limosilactobacillus fermentum*	2	*Lactobacillus casei/paracasei/rhamnosus*	2	22	M8	*Limosilactobacillus reuteri*	2		
8	MI	*Lactobacillus acidophilus/gasseri*	2	*Limosilactobacillus fermentum*	4	23	M9	*Lactobacillus acidophilus/gasseri*	3		
9	ML	*Limosilactobacillus fermentum*	3	*Lactobacillus acidophilus/gasseri*	3	24	M10	*Lactobacillus acidophilus/gasseri*	3		
10	MN	*Limosilactobacillus reuteri*	2	*Lactobacillus acidophilus/gasseri*	2	25	M11	*Lactobacillus acidophilus/gasseri*	4		
11	MO	*Lactobacillus acidophilus/gasseri*	3			26	M12	*Lactobacillus acidophilus/gasseri*	5		
12	MP	*Lactobacillus casei/paracasei/rhamnosus*	3			27	M13	*Lactobacillus casei/paracasei/rhamnosus*	2		
13	MR	*Lactobacillus acidophilus/gasseri*	2	*Lactobacillus casei/paracasei/rhamnosus*	3	28	M14	*Lactobacillus casei/paracasei/rhamnosus*	5		
14	MS	*Lactobacillus acidophilus/gasseri*	3			29	M15	*Lactobacillus acidophilus/gasseri*	2		
15	M1C	*Lactobacillus acidophilus/gasseri*	4			30	M16	*Lactobacillus casei/paracasei/rhamnosus*	3		

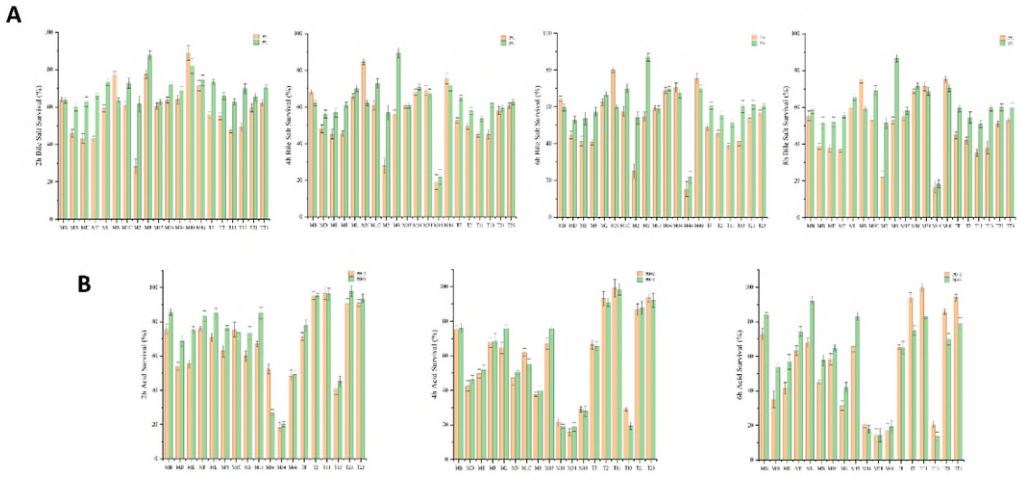
number	Study identifier	Identification results	number of positive results	Identification results	number of positive results	number	Study identifier	Identification results	number of positive results	Identification results	number of positive results
31	M17	*Limosilactobacillus fermentum*	1	*Lactobacillus casei/paracasei/rhamnosus*	2	46	M35	*Lactobacillus casei/paracasei/rhamnosus*	2		
32	M19	*Limosilactobacillus fermentum*	2			47	M36	*Lactobacillus casei/paracasei/rhamnosus*	4		
33	M20	*Lactobacillus casei/paracasei/rhamnosus*	3			48	M37	*Lactobacillus casei/paracasei/rhamnosus*	3		
34	M21	*Limosilactobacillus fermentum*	3	*Lactobacillus casei/paracasei/rhamnosus*	3	49	M38	*Lactobacillus casei/paracasei/rhamnosus*	3		
35	M22	*Lactobacillus acidophilus/gasseri*	2	*Lactobacillus casei/paracasei/rhamnosus*	3	50	M39	*Lactobacillus casei/paracasei/rhamnosus*	3		
36	M24	*Limosilactobacillus reuteri*	3	*Lactobacillus casei/paracasei/rhamnosus*	2	51	M40	*Lactobacillus casei/paracasei/rhamnosus*	3		
37	M25	*Limosilactobacillus fermentum*	2			52	M44	*Enterococcus gallinarum*	1	*Lactobacillus casei/paracasei/rhamnosus*	3
38	M26	*Lactobacillus acidophilus/gasseri*	3	*Lactobacillus casei/paracasei/rhamnosus*	4	53	M46	*Lactobacillus casei/paracasei/rhamnosus*	4		
39	M28	*Lactobacillus acidophilus/gasseri*	1	*Lactobacillus casei/paracasei/rhamnosus*	6	54	M47	*Lactobacillus acidophilus/gasseri*	2	*Lactobacillus casei/paracasei/rhamnosus*	2
40	M29	*Lactobacillus acidophilus/gasseri*	3	*Limosilactobacillus fermentum*	1	55	M49	*Lactobacillus casei/paracasei/rhamnosus*	2	*Lactobacillus acidophilus/gasseri*	1
41	M30	*Lactobacillus acidophilus/gasseri*	2			56	M50	*Lactobacillus casei/paracasei/rhamnosus*	3	*Lactobacillus acidophilus/gasseri*	1
42	M31	*Lactobacillus casei/paracasei/rhamnosus*	6			57	M51	*Lactobacillus casei/paracasei/rhamnosus*	1	*Lactobacillus acidophilus/gasseri*	3
43	M32	*Lactobacillus casei/paracasei/rhamnosus*	4			58	M52	*Lactobacillus casei/paracasei/rhamnosus*	3		
44	M33	*Lactobacillus casei/paracasei/rhamnosus*	3	*Limosilactobacillus reuteri*	1	59	M53	*Lactobacillus casei/paracasei/rhamnosus*	4		
45	M34	*Lactobacillus casei/paracasei/rhamno*	3			60	M1D	*Lactobacillus*	4		

number	Study identifier	Identification results	number of positive results	Identification results	number of positive results	number	Study identifier	Identification results	number of positive results	Identification results	number of positive results
61	TC	*Lactobacillus acidophilus/gasseri*	2			77	T14	*Lactobacillus acidophilus/gasseri*	3	*Limosilactobacillus fermentum*	1
62	TD	*Lactobacillus acidophilus/gasseri*	4			78	T15	*Lactobacillus acidophilus/gasseri*	2	*Limosilactobacillus fermentum*	2
63	TE	*Lactobacillus acidophilus/gasseri*	2	*Lactobacillus casei/paracasei/rhamnosus*	2	79	T16	*Lactobacillus acidophilus/gasseri*	2		
64	TF	*Lactobacillus acidophilus/gasseri*	2	*Lactobacillus casei/paracasei/rhamnosus*	2	80	T17	*Lactobacillus acidophilus/gasseri*	2	*Limosilactobacillus fermentum*	1
65	T1	*Lactobacillus acidophilus/gasseri*	2			81	T18	*Lactobacillus acidophilus/gasseri*	2		
66	T2	*Lactobacillus acidophilus/gasseri*	4			82	T19	*Lactobacillus acidophilus/gasseri*	4	*Limosilactobacillus fermentum*	1
67	T3	*Lactobacillus acidophilus/gasseri*	4			83	T20	*Lactobacillus acidophilus/gasseri*	2	*Lactobacillus casei/paracasei/rhamnosus*	2
68	T4	*Lactobacillus acidophilus/gasseri*	4			84	T21	*Lactobacillus acidophilus/gasseri*	2		
69	T5	*Lactobacillus acidophilus/gasseri*	4			85	T22	*Lactobacillus acidophilus/gasseri*	2		
70	T6	*Lactobacillus acidophilus/gasseri*	2	*Lactobacillus casei/paracasei/rhamnosus* 50%+*Lactobacillus acidophilus/gasseri* 50%	1	86	T23	*Lactobacillus acidophilus/gasseri*	2	*Lactobacillus casei/paracasei/rhamnosus*	3
71	T7	*Lactobacillus acidophilus/gasseri*	2	*Lactobacillus casei/paracasei/rhamnosus*	2	87	BD	*Enterococcus gallinarum*	2		
72	T8	*Lactobacillus acidophilus/gasseri*	2			88	B1	*Escherichia coli*	4	*Enterococcus gallinarum*	3
73	T10	*Lactobacillus acidophilus/gasseri*	2			89	B5	*Enterococcus gallinarum*	4		
74	T11	*Lactobacillus acidophilus/gasseri*	2			90	B6	*Enterococcus gallinarum*	4		
75	T12	*Lactobacillus acidophilus/gasseri*	2			91	B7	*Enterococcus gallinarum*	4		
76	T13	*Lactobacillus acidophilus/gasseri*	2								

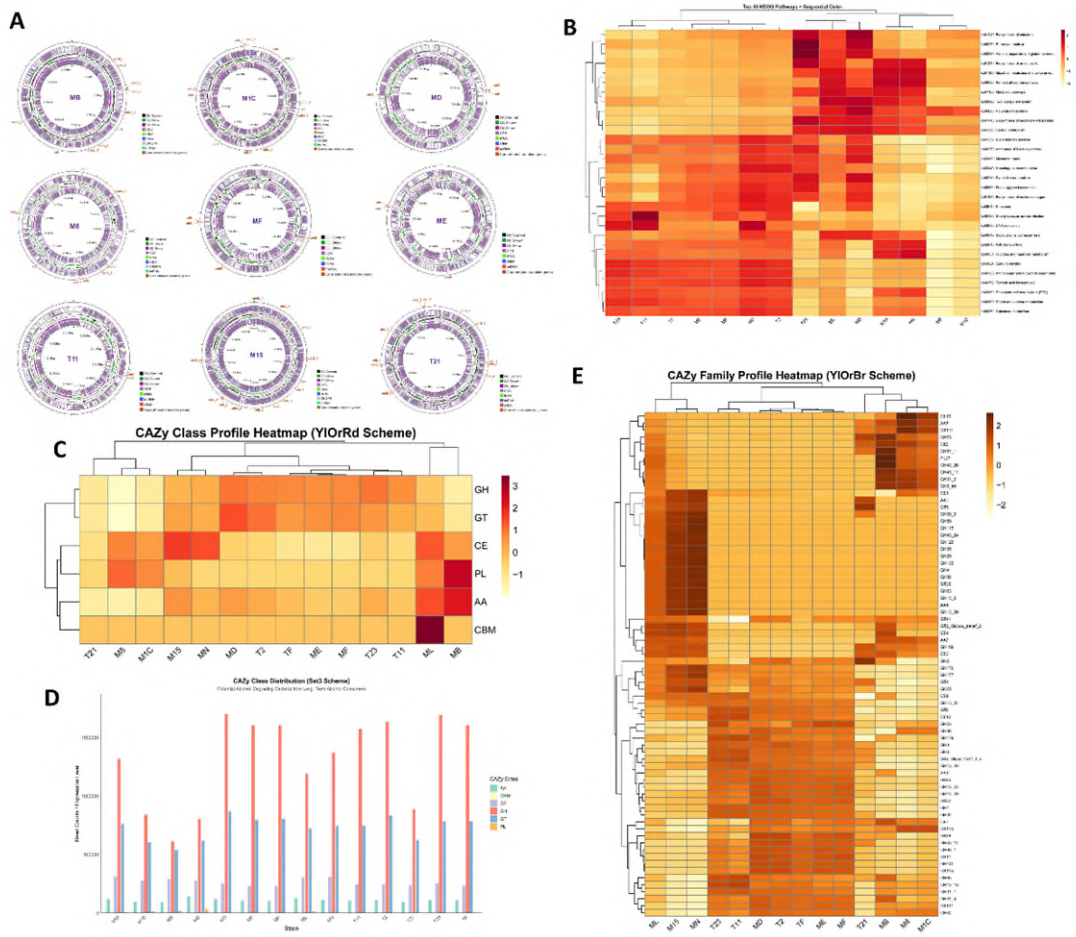
S 1. Taxonomic identification results of 91 purified bacterial isolates using mass pectrometry.



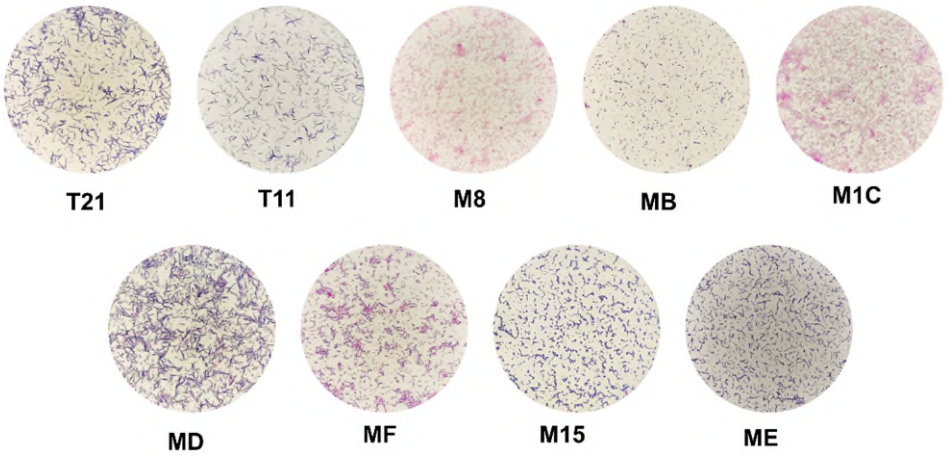
S 2. Time-course analysis of ethanol degradation rate over 48 hours for 91 purified bacterial isolates.



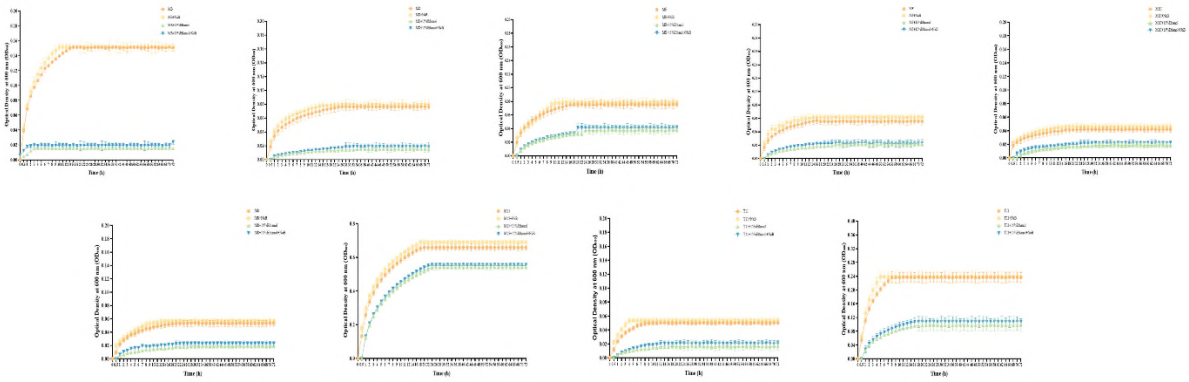
S 3. Additional data supporting gastrointestinal stress tolerance screening.



S 4. Genomic and functional annotation of other candidate strains.



S 5 Gram staining of other candidate strains.



S 6 Growth curves of other candidate isolates under ethanol-free and ethanol-stressed (15%) conditions, with or without NaB supplementation.